Transition from passive to active rifting: Relative importance of asthenospheric doming and passive extension of the lithosphere

Article *in* Journal of Geophysical Research Atmospheres · June 2001

DOI: 10.1029/2000JB900424

CITATIONS
171

READS
186

3 authors, including:

Ritske Huismans
University of Bergen
116 PUBLICATIONS **3,151** CITATIONS

SEE PROFILE

JOURNAL OF GEOPHYSICAL RESEARCH, VOL. 106, NO. B6, PAGES 11,271–11,291, JUNE 10, 2001

Transition from passive to active rifting: Relative importance of asthenospheric doming and passive extension of the lithosphere

Ritske S. Huismans[1]
Institute of Earth Sciences, Vrije Universiteit, Amsterdam, Netherlands

Yuri Y. Podladchikov
Geologisches Institut, ETH-Zentrum, Zurich, Switzerland

Sierd Cloetingh
Institute of Earth Sciences, Vrije Universiteit, Amsterdam, Netherlands

Abstract. We present quantitative modeling results of the dynamic interplay of passive extension and active convective thinning of the mantle lithosphere beneath intracontinental rift zones investigating the relative importance of thermal buoyancy forces associated with asthenospheric doming and far-field intraplate stresses on the style of rifting. To this aim we employ a twodimensional numerical code based on a finite element method formulation for nonlinear temperature dependent viscoelastoplastic rheology. Brittle behavior is modeled using Mohr-Coulomb plasticity. The models support a scenario in which passive stretching leads to an unstable lithospheric configuration. Thermal buoyancy related to this asthenospheric doming subsequently drives active upwelling in a lithosphere scale convection cell. In the late synrift to early postrift the lithospheric horizontal stresses caused by the active asthenospheric upwelling may start to compete with the far-field intraplate stresses. At this stage the domal forces may dominate and even drive the system causing a change from passive to active rifting mode. If this transition occurs, the model predicts (1) drastic increase of subcrustal thinning beneath the rift zone, (2) lower crustal flow towards the rift flanks, (3) middle crustal flow towards the rift center, (4) the coeval occurrence of tensional stresses within and compressive stresses around the upwelling region, and (5) possible surface uplift. Late postrift thermal cooling removes the thermal buoyancy forces. At this stage the far-field forces dominate the stress state again and the lithosphere becomes more sensitive to small changes in the intraplate stresses. The model results may explain several key observations that are characteristic of a large number of intracontinental rift basins. These features include differential thinning of extending lithosphere, the discrepancy between fault-related extension and crustal thinning, late (end of synrift to early postrift) mantle related volcanism, surface domal uplift succeeding rifting, and rift flanks uplift associated with extension of a weak lithosphere.

1. Introduction

Thinning of the lithosphere, rifting and continental breakup have long been considered in terms of two end-member groups of models: active rifting models and passive rifting models (Figure 1) [*Sengor and Burke,* 1978; *Turcotte and Emerman,* 1983]. In the first group, convective upwelling of the asthenosphere drives rifting, e.g., a mantle plume impinging on the base of the lithosphere drives continental breakup. In these models, local buoyancy forces generate the tensional stresses able to break the lithosphere [*Houseman and England,* 1986]. In the second group of models, horizontal, in-plane far-field forces, possibly due to large-scale plate interactions, initialize and drive lithosphere extension and rifting [*Cloetingh and Wortel,* 1986].

The relative timing of rifting and rift-related volcanism was used to discriminate between these two basic

[1]Now at Department of Oceanography, Dalhousie University, Halifax, Nova Scotia, Canada.

Paper number 2000JB900424.
0148-0227/01/2000JB900424$09.00

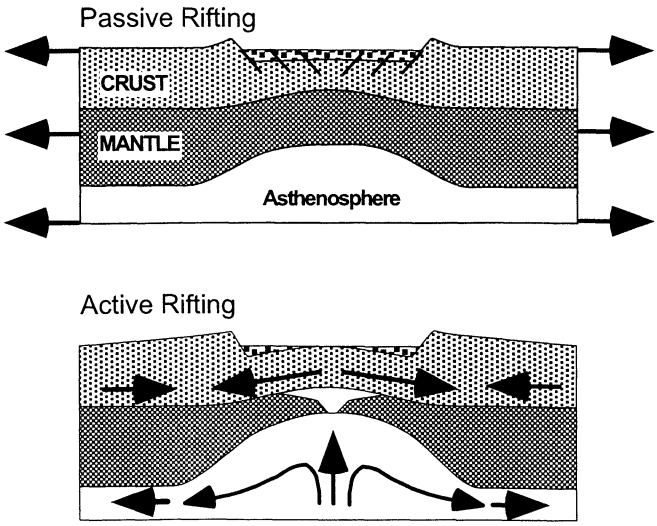

Figure 1. End-member models of rifting *Sengor and Burke,* [1978]. Passive rift models in which the driving forces are given by far-field extensional stresses and the space created by lithosphere thinning is passively filled by the asthenosphere. In passive models the crust and mantle are expected to thin in a homogeneous way, and volcanism and doming are expected to postdate rifting. Active rift models in which the driving forces providing for extension are generated by active mantle plume impingement on the base of the lithosphere. In active models the crust and mantle are not necessarily thinning in a homogeneous way, i.e., subcrustal thermal erosion of the mantle lithosphere may be envisaged, volcanism and doming are expected to precede rifting.

types of rifting [*Sengor and Burke,* 1978]. In rift zones where doming and volcanism precede rifting, an active mantle plume was believed to act on the base of the lithosphere. In contrast, in rift zones where volcanism and doming succeed rifting, the asthenosphere was assumed to play a passive role, filling the space created by localized extension. *Sengor and Burke* [1978] stated that the passive mode of rifting is by far the more widespread of the two. The following observations support this conclusion:

1. Mantle plume-related uplift preceding rifting is rarely observed in the stratigraphic record [*Sengor and Burke,* 1978; *Ziegler,* 1994]. On the contrary, a number of rift basins and rifted continental margins show widespread doming 20 to 60 Myr after the beginning of extension [*Ziegler,* 1994; *Horvath and Cloetingh,* 1996; *Delvaux et al.,* 1997]. Uplift of synrift grabens to 2 km above sealevel attest to these late vertical movements [*Karner et al.,* 1992; *Ziegler,* 1994].

2. Rift-related shallow asthenospheric volcanism occurs, if at all, late in the synrift and/or postrift evolution [*Latin and Waters,* 1991; *Wilson,* 1993]

3. Rift-related volcanism has a generally enriched upper asthenosphere or mantle lithosphere signature, which is not typical for mantle plume-derived magmas [*Wilson,* 1993].

Indeed, a number of observations (i.e., Table 1) suggest that neither of the two end-member models adequately describes real-world rifts. Typically, the observations 1-3 work well in rejecting the active mode of rifting, but the magnitude of the postrift doming, the high amount of shallow mantle volcanism [*White and McKenzie,* 1989; *Latin and Waters,* 1991; *Keen et al.,* 1994], and the strong differential thinning of the lithosphere [*Royden and Keen,* 1980; *Beaumont et al.,* 1982] are difficult to explain with models of pure shear extension driven by far-field forces alone.

Application of the original McKenzie model [*McKenzie,* 1978] to extensional basins showed substantial deviations from the model predictions [*Royden and Keen,* 1980; *Sclater et al.,* 1980; *Beaumont et al.,* 1982; *Kooi,* 1991]. In order to explain minor or absent synrift subsidence and/or very high subsidence in the postrift in for instance the North Sea, the Labrador Sea, the Pannonian basin, and many other basins, the differential stretching model was proposed [*Royden and Keen,* 1980; *Beaumont et al.,* 1982] in which the crust and the mantle lithosphere are allowed to thin by different amounts. In general, additional subcrustal heating, i.e., mantle lithosphere thinning in the late synrift/postrift is needed to predict the observed basin stratigraphy.

The listed observations point to latestage activity in the mantle lithosphere/asthenosphere in the evolution of rifted basins. These features characterize among others the central North Sea basin (Figure 2) [*Kooi,* 1991], Upper Rhine graben [*Ziegler,* 1995], the Pannonian basin [*Royden et al.,* 1983; *Horvath,* 1993; *Huismans,* 1999], the North Tyrrhenean sea [*Bartole,* 1995], the North Atlantic passive margins [*Keen et al.,* 1994], Lake Baikal (Figure 3) [*Delvaux et al.,* 1997], the Gulf of Lyon and the Valencia trough [Bois, 1993], the Alboran Sea [*Cloetingh et al.,* 1995] and the Rio Grande rift zone (Figure 3) [*Davies,* 1991] (see also Table 1).

The discrepancy between the predictions of passive rift models and the observations may be solved by active destabilization of the mantle lithosphere in response to the previous passive rift history. The density of the asthenosphere and the mantle lithosphere is predominantly governed by the thermal expansion of the rocks. As a consequence, the mantle lithosphere is in a gravitationally unstable situation (Figure 4). This potential instability has been the subject of various proposed mechanisms for mantle lithosphere thinning, among others, mantle delamination [*Bird,* 1978], boundary layer instability [*Houseman et al.,* 1981], and diapiric upwelling of the asthenosphere in a small-scale convective mode [*Marechal,* 1983; *Buck,* 1985; *Keen,* 1985; *Buck,* 1986; *Dunbar and Sawyer,* 1988; *Keen and Boutilier,* 1995; *Huismans,* 1999]. The potential of the instability grows with increasing perturbation. Therefore perturbations created by (mainly) horizontal plate tectonic deformations have the tendency to be amplified with time and in the case of passive lithospheric thinning, active upwelling of the asthenosphere with all related

Table 1. Features of Pannonian Basin, Baikal Rift, Oslo Graben, and Other Sedimentary Basins[a]

Basins	β	δ	First Rift Phase, Myr	Second Rift Phase, Myr	Calc Alkaline Volcanics, Myr	Alkaline Volcanics, Myr
Pannonian Basin	1.6-1.8	8-10	18-14	12-11	18-6	12-0
Baikal rift	1.4-1.6	3-4(?)	24- 6	4-0	?	20-14
Oslo Graben	1.3-1.4	4-5	300-270	270-240	?	280-270
North Sea	1.3-1.6	5-5.5	248-219	166-118	?	176-163
Upper Rhine Graben	1.1-1.2	3-5(?)	40-23	18-0(?)	?	12-0
Limagne Graben	1.2-1.3	3-5(?)	36-23	10-5	?	12-0
Gulf Lyon Margin	1.2-2.0	3(?)	23-16	?	36-30	12-0
Valencia trough	1.2-2.0	4-5	23-16	?	23-18	10-0
Alboran Sea	1.5-2.5	4-8	23-16	9-5	?	10-0
Dnepr Don Basin	1.1-1.5	1.1-10	370-362	345-340	?	363

Basins	Postrift Unconformity	Postrift Doming	First Rift Phase	Second Rift Phase	Coeval Ext. Contr.	Reference
Pannonian Basin	yes	12-11 Myr	T tension	P tension	yes	1,2
Baikal rift	?	0 Myr	T tension	P tension	?	3,4
Oslo Graben	yes	240-220 Myr	T tension	P tension	?	5
North Sea	yes	183-156 Myr	P tension	R tension	yes (?)	6,7,8
Upper Rhine Graben	?	10-0 Myr	P tension	T tension	?	9,10
Limagne Graben	?	12-0 Myr	T tension	?	?	10
Gulf Lyon Margin	no	no	P tension	?	?	10,11
Valencia Trough	?	15-0(?) Myr	P tension	?	yes	10,12
Alboran Sea	?	11 Myr	T tension	P tension	yes	13,14
Dnepr Don Basin	?	330 Myr	P tension	P tension	?	15,16

[a]Basin features β and δ are crustal and subcrustal thinning respectively. Timing of rift phases, volcanism, and postrift doming are given in absolute ages in Myr. Stress regime for the first and second rift phase, T tension is trans tension, P tension is pure tension, R tension is radial tension, and Coeval Ext. Contr. is coeval extension and contraction. References are 1, *Royden et al.* [1983]; 2, *Horvath* [1993]; 3, *Zorin* [1981]; 4, *Delvaux et al.* [1997]; 5, *Heeremans et al.* [1996]; 6, *Ziegler* [1992]; 7, *Latin and Waters* [1991]; 8, *Kooi* [1991]; 9, *Ziegler* [1995]; 10, *Bois* [1993]; 11, *Kooi et al.* [1992]; 12, *Janssen et al.* [1993]; 13, *de Ruig* [1992]; 14, *Weijermars* [1991]; 15, *van Wees et al.* [1997]; 16, *Wilson and Lyashkevich* [1996].

features is expected to follow the first passive rift event (Figure 5). Here the term active rifting is used in the sense of buoyant asthenospheric upwelling not necessarily implying the involvement of a deep mantle plume. Thus the small-scale convective instability of the mantle lithosphere may solve the (apparent) discrepancy between passive rift models and observations.

We employ fully dynamic two-dimensional finite element modeling to study the feedback mechanism between the thinning of the lithosphere induced by far-field forces and local buoyancy flows modifying rift basin morphology. In order to circumvent the limitations of previous models, thermal buoyancy forces and nonlinear temperature-dependent viscoelastoplastic rheology are incorporated. The key questions we try to solve are as follows:

1. Which conditions favor significant diapiric upwelling and the development of an active stage?

2. What are the stresses generated by an asthenospheric dome and how will they compare with far-field stresses and the strength of the lithosphere?

We will first use simple analytical models to estimate the amount of rift push force generated upon lithospheric thinning. Subsequently, a two-dimensional finite element model will be used to perform a series of numerical experiments on the sensitivity of mantle lithosphere destabilization to the thermomechanical structure of the lithosphere and to far-field imposed deformation.

2. Rift Push Forces Owing to Two-Stage Thinning of the Lithosphere

Deformation of the lithosphere changes the lateral and vertical distribution of crust and mantle lithosphere materials and the temperature structure of the lithosphere, which both will create lateral and vertical density variations. These generate buoyancy forces (F_B) that tend to bring the lithosphere into a laterally homogeneous and vertically stable state [*Artyushkov,* 1973]. Under the assumption that density anomalies create topography in local isostatic equilibrium the buoyancy

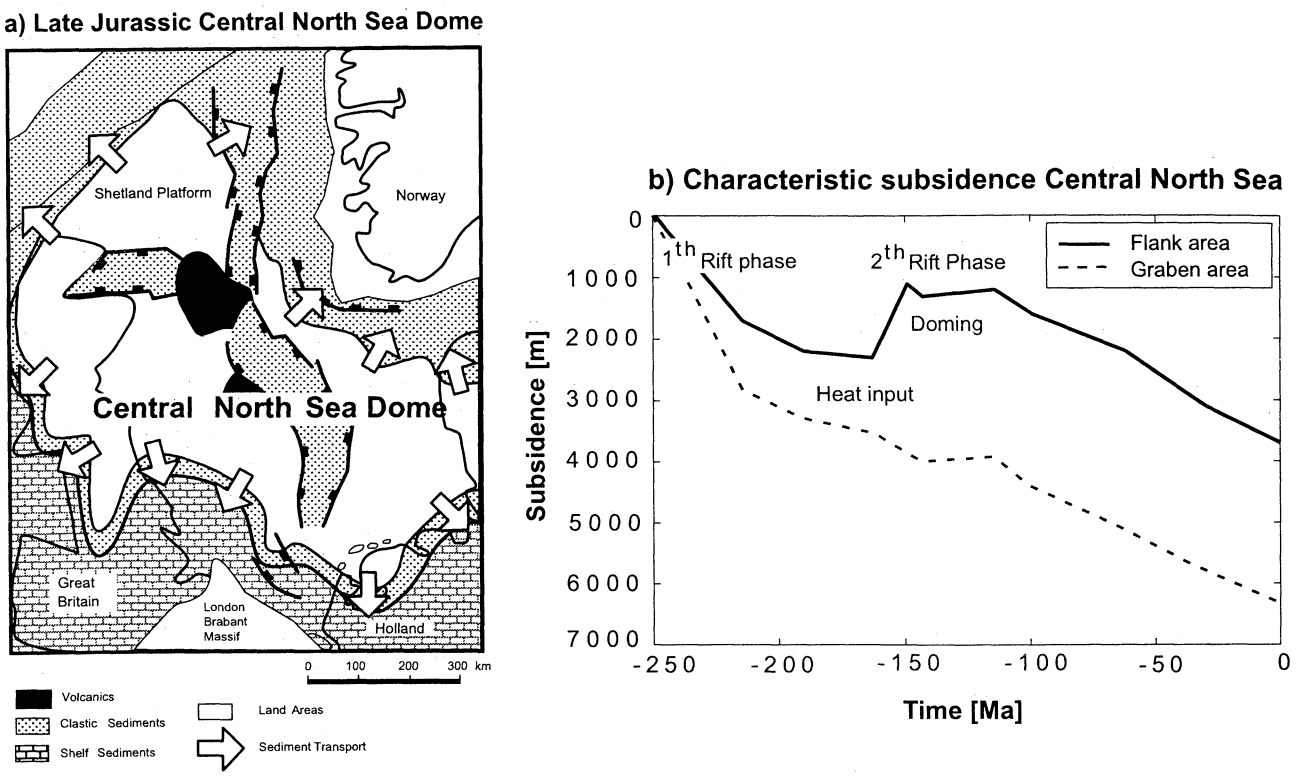

Figure 2. (a) North Sea basin features [after *Kooi,* 1991; *Ziegler,* 1992]: extent of the middle to late Jurassic central North Sea dome and broad arch uplift affected the central North Sea in the mid-Jurassic (183-156 Myr). The amount of uplift is of the order of 0.5-2.5 km. The doming is associated with a large volcanic center (solid area) at the triple junction of the graben system. Alkaline volcanism is related to decompression melting of the shallow asthenosphere. The subsidence analysis, the doming, and the decompression melts show that the second rift phase was dominated by the effects of mantle lithosphere thinning. (b) Characteristic subsidence curves of the North Sea basin [after *Kooi,* 1991] is given for two wells in 2-D best fit forward modeled stratigraphy. The solid curve gives the subsidence history of the flank region, whereas the dashed curve gives the subsidence history of the graben area. The rift evolution is characterized by a first rift phase in the Late Triassic-Early Jurassic (248-219 Myr) with homogeneous extension. In the mid-Jurassic (166-148 Myr) strong doming occurred due to subcrustal thinning with estimated relief of 0.5-2 km. Prior to the doming, most alkaline volcanics erupted. A second rift phase with strong subcrustal thinning and minor crustal extension is placed in the Late Jurassic-Early Cretaceous (163-118 Myr). Stretching was nonuniform, especially for the second rift phase. Subcrustal heating is needed to limit the amount of postrift subsidence.

force can be obtained by integrating the pressure difference with depth [*Fleitout and Froidevaux,* 1982; *Le Pichon and Alvarez,* 1984]:

$$F_{\text{Buoyancy}} = \int_0^{Z_{\text{compensation}}} \Delta\rho(z) g z dz = \int_0^{Z_{\text{compensation}}} \Delta P(z) dz. \quad (1)$$

There are two components to these pressure differences:

1. Crustal thinning produces a low lithostatic pressure in the lower crust at the rift axis with respect to the thicker flanking regions due to the lower weight of the overlying column of crustal rocks. The effect is that lower crustal material tends to flow inward from the sides of the rift zone (Figure 6a).

2. Thinning of the mantle lithosphere and uplift of the Moho at the rift axis generate a high lithostatic pressure in the thinned column with respect to the flanking areas. The light asthenospheric material has the tendency to flow upward and sideward to replace colder and denser mantle lithospheric material in a diapiricmode. Furthermore, the lower crust tends to flow toward the flanking regions in reaction to the Moho uplift.

The buoyancy forces due to crustal and mantle lithosphere thinning are thus of opposite sign. Although the density contrast between crust and mantle is much larger than the density change due to the temperature variations in the mantle lithosphere, the contribution of the latter can be much larger because of the greater depth extent of the mantle lithosphere.

As shown by *Turcotte and Emerman* [1984] and *Le Pichon and Alvarez* [1984], the buoyancy force, owing to

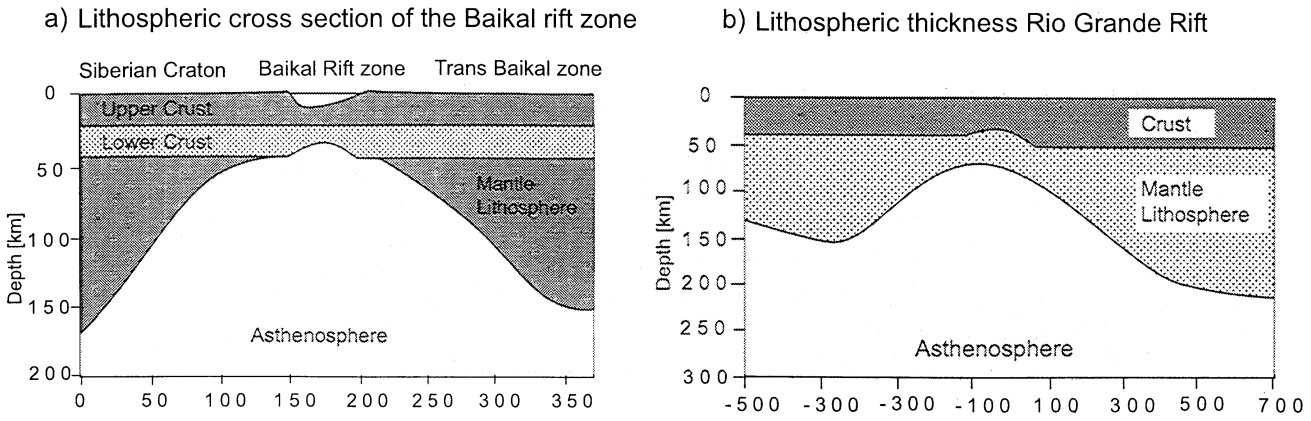

Figure 3. (a) Lithosphere structure over the Rio Grande rift zone as documented by teleseismic travel time residuals [after *Davies,* 1991]. Mantle tomography over the Rio Grande rift zone shows strong mantle lithosphere thinning beneath the rift zone from values of 150 to 200 km under the stable shield to 75 km under the rift zone whereas the crust is thinned by a minor amount. (b) Lithospheric cross section over the Baikal rift zone [after *Zorin,* 1981]. Mantle tomography shows strong upwelling of the asthenosphere beneath the Baikal rift zone. Evidence shows that mantle lithosphere thinning occurred recently, e.g., late in the rift history [*Delvaux,* 1997].

lithosphere thinning by a factor 2 (Figure 6a), is of the order of 2 x 10^{12} N m^{-1} (Figure 6b). In case of continental rifting, this results in most cases in a net rift push force analogous to the ridge push force, which makes rifting a self-propagating process where the rift push force has the tendency to accelerate the rifting process, making it an inherently unstable process. With relaxation of the thermal anomaly a decrease takes place of the tensional component of F_B, and the rift push force eventually reverses sign, giving way to compression in the late postrift [*Le Pichon and Alvarez,* 1984].

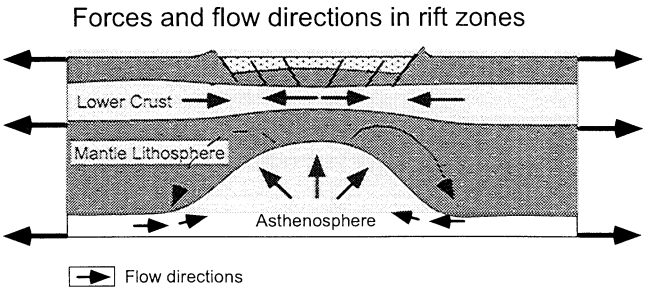

Figure 4. Far-field forces and buoyancy forces due to crust as well as lithosphere thinning and their related potential flow directions. Because of the density inversion over the lithosphere-asthenosphere boundary following a passive rift event, active upwelling of the asthenosphere is expected to occur in the late synrift/early postrift. Buoyancy forces due crustal thinning tend to drive lower crustal flow toward the rift zone, whereas the buoyancy forces due mantle lithosphere thinning, Moho uplift, and possible dynamic pressures due to upwelling of the asthenosphere beneath the basin have the tendency to drive the lower crust toward the rift flanking areas. In the synrift and early postrift, outward flow dominates whereas in the late postrift inward flow may occur.

If we consider a situation where, following a first passive rift phase, additional thinning of the mantle lithosphere occurs in the late synrift to early postrift, the tensional buoyancy forces may increase dramatically. The density distribution in the rift system is significantly changed by the additional mantle lithosphere thinning. Consequently the thinned area is uplifted to lower elevations (Figure 7). This has the effect of decreasing and eventually diminishing the compressional component and increasing the rift push component of the integrated buoyancy force.

The simple model used above to estimate the buoyancy forces upon lithosphere thinning is employed to estimate the increase of the buoyancy force owing to late synrift/early postrift additional mantle lithosphere thinning. The crust is thinned by a fixed amount, whereas mantle lithosphere thinning is varied between the initial fixed amount and complete removal (Figure 8). At the start, upon homogeneous thinning, the rift push force is in the range 1 x 10^{11} – 1.45 x 10^{11} N m^{-1} (Figure 8), whereas it increases to maximum values of 1.85 x 10^{12} – 2.2 x 10^{12} N m^{-1} upon subsequent lithosphere thinning.

The integrated yield strength of the lithosphere depends strongly on the thermal structure of the lithosphere and the crustal thickness [*Cloetingh et al.,* 1995]. The horizontal force needed to cause significant extensional yielding of the lithosphere can be estimated by integrating the yield stress with depth. The extensional strength of lithosphere (F_s) with a typical surface heat flow of $q_s = 50$ x 10^{-3} W m^{-2} is of the order $F_s \sim 3$ x 10^{13} N m^{-1}, whereas with a surface heat flow of $q_s \geq 75$ x 10^{-3} W m^{-2} the force may be less than $F_s \sim 1$ x 10^{12} N m^{-1} [*Kusznir,* 1982]. Since for most rift basins the surface heat flow $q_s > 75$ x 10^{-3} W m^{-2} [*Vitorello and*

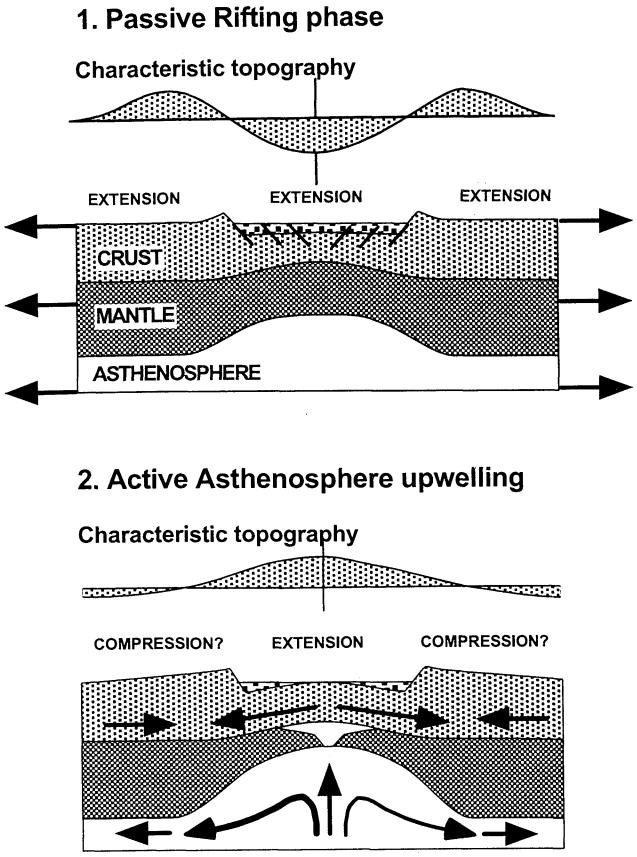

Figure 5. Transition from passive to active rifting due to small-scale convective destabilisation of the mantle lithosphere in the late synrift/early postrift. A hybrid alternative to the end-member models of rifting is shown. Doming and shallow asthenosphere volcanism are expected to occur in the late synrift/early postrift eventually associated with a second rift phase.

Pollack, 1980; *Morgan and Sass,* 1984], we envisage that the buoyancy forces owing to lithosphere thinning may well be sufficient to cause significant failure and to drive a second phase of extension.

According to the estimates given above for the buoyancy forces due to lithosphere thinning twostage development of rifting is predicted. The predicted stress levels are sufficient to produce a second phase of extension. In addition, the rift push force will generate not only tension in the rifted area itself but will also generate compression toward the flanking areas of the rift zone thus showing a pattern of coeval tension and compression. This may explain the frequent observation of laterally changing stress state in arc-backarc environments and the occurrence of coeval extension and contraction in these settings (see Table 1 and *Cloetingh et al.* [1995]). Thus small-scale convective thinning of the mantle lithosphere may result in a drastic increase of the rift push force with stress levels of the order of plate boundary forces.

3. Numerical Method

We simulate lithosphere extension using the finite element method. A new numerical code has been developed which is based on extension of a twodimensional finite element formulation for viscous incompressible flow [*Poliakov and Podladchikov,* 1992]. We modified the existing viscous code, adding elastic, plastic, and nonlinear viscous behavior and supplemented it with a thermal routine calculating the thermal field during run time. The implementation involves solving the static equilibrium equations:

$$\frac{\partial \sigma_{ij}}{\partial x_j} + \rho g_i = 0, \tag{2}$$

where σ_{ij} is the stress tensor, ρ is the density, g_i is the gravity acceleration, and repeating indexes imply summation. The deviatoric deformation below plastic yield is governed by Maxwell viscoelastic rheology:

$$\dot{e}_{ij} = \frac{\dot{\tau}}{2G} + \frac{\tau_{ij}}{2\mu_{\text{eff}}}. \tag{3}$$

Here $\dot{e}_{ij}$ is the deviatoric strain rate tensor, τ_{ij} is the deviatoric stress tensor, G is the elastic shear modulus, μ_{eff} is the effective viscosity, and $\dot{\tau}$ is the objective Jaumann stress rate [*Hughes and Winget,* 1980]. Taking the first-order backward difference in time of the deviatoric stress results in

$$\tau_{ij} = \eta \dot{e}_{ij} + \eta\theta\tau_{ij}^{\text{old}}, \tag{4}$$

where η represents an effective viscosity for viscoelastic flow, $\eta = 1/(1/\mu_{\text{eff}} + 1/\Delta tG)$, with μ_{eff} the effective viscosity, $\theta = 1/2\Delta tG$ and the supscript old refers to the previous time step value. The volumetric deformation of the material is elastic:

$$\frac{\partial P}{\partial t} = -K\dot{e}_{ii} = -K\nabla\mathbf{v}, \tag{5}$$

where K is the bulk elastic modulus and $\nabla\mathbf{v}$ is the divergence of velocity. The first order backward difference is given by

$$P = P^{\text{old}} - \Delta tK\nabla\mathbf{v}. \tag{6}$$

Now, since $\sigma_{ij} = -P\delta_{ij} + \tau_{ij}$, we can substitute the discretized forms of the constitutive relationships (4) and (6) into the static equilibrium equation (2) which yields

$$\nabla_j(2\eta\dot{e}_{ij}) + \nabla_i\left(\frac{\Delta tK}{3}\nabla\mathbf{v}\right) = \nabla_i P^{\text{old}} - \rho g_i - \nabla_j(\eta\theta\tau_{ij}). \tag{7}$$

The system of three equations (6) and (7) for three unknown functions P, v_x and v_y is identical to one for

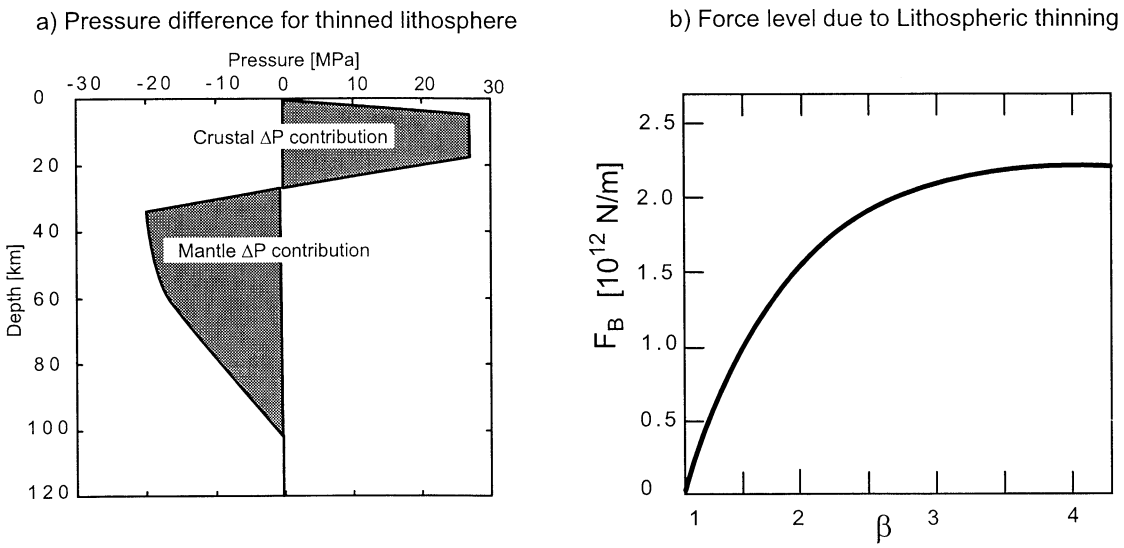

Figure 6. (a) Illustration of buoyancy force F_B due to lithosphere thinning under the assumption of local isostasy [after *le Pichon and Alvarez,* 1984; *Turcotte and Emerman,* 1983]. F_B is given by the integrated pressure difference with depth. Homogeneous thinning of reference lithosphere of 10 km thick with a 35-km-thick crust by a factor of $\beta = 2$. The contribution due to mantle thinning is larger then the contribution resulting from crustal thinning. This results in a net tensional rift push force of the order of 1 x 10^{12} N m^{-1}. Average densities are used, no account is made of the thermal structure of the lithosphere. Crustal density is 2900 kg m^{-3}, mantle lithosphere density is 3360 kg m^{-3}, asthenosphere density is 3300 kg m^{-3}, and infill of thinned area by sediment of density 2400 kg m^{-3}. (b) Tensional stress level due to lithosphere thinning [after *Turcotte and Emerman,* 1983]. Buoyancy forces are calculated by thinning a reference lithosphere of 120 km thick with a 35-km-thick crust taking account the thermal structure of the lithosphere under the assumption of local isostasy. By concentrating the buoyancy force in an elastic plate of 50 km thick, stress levels result of the order of 40-60 MPa.

viscous incompressible media. The only modification required for existing penalty primitive variables FEM formulation [*Poliakov and Podladchikov,* 1992] is that for the right-hand side vector, providing that the new definition of the effective viscosity is used. Consecutive updates of the stress components must be done to discretize in time equations (3) and (5), e.g., using equations (4) and (6).

The effective viscosity depends on the current strain rate and temperature:

$$\mu_{\text{eff}} = \left(\frac{3^{\frac{(n+1)}{2}}}{2}A\right)^{-\frac{1}{n}} \sqrt{\dot{E}_{2D}}^{\frac{(1-n)}{n}} \exp(Q/nRT), \quad (8)$$

where T is temperature, $\dot{E}_{2D}$ is the second invariant of the deviatoric strain rate tensor, Q is the activation energy, n is the power law exponent, and R is the gas constant. This type of power law rheology is supported by laboratory experiments [*Carter and Tsenn,* 1987]. The values of A, Q, n we chose to correspond to those for an olivine mantle, a diabase lower crust and a dry granite upper crust [*Carter and Tsenn,* 1987] (Table 2).

Brittle deformation is modeled with an elastoplastic rheology. Plastic flow occurs depending on whether a plastic yield criterion is satisfied. The yield envelope is described by the Mohr-Coulomb criterion for brittle failure in terms of principal stresses:

$$F = \sigma_1 - \sigma_3 N_\Phi + 2C\sqrt{N_\Phi}, \quad (9)$$

where $N_\Phi = (1 + \sin\Phi)/(1 - \sin\Phi)$, σ_1 is the maximum and σ_3 is the minimum principal stress, Φ is the friction angle, and C is the cohesion. The angle of internal friction is setup to follow Byerlee's law (Φ = 30°-40°). If the state of stress lies outside the failure envelope, i.e., $F \leq 0$, plastic flow occurs and stress is reduced according to an associative or nonassociative flow law. Constitutive plastic stress-strain relationships can be derived using the plastic potential G [*Cundall and Board,* 1988]:

$$G = \sigma_1 - \sigma_3 N_\Psi, \quad (10)$$

where $N_\Psi = (1 + \sin\Psi)/(1 - \sin\Psi)$, and Ψ is the dilatation angle. Note that in nonassociative flow $\Phi \neq \Psi$. The increments of plastic strains in principal stress directions are given by

$$\Delta e_i^{\text{plastic}} = \lambda_s \frac{\partial G}{\partial \sigma_i}. \quad (11)$$

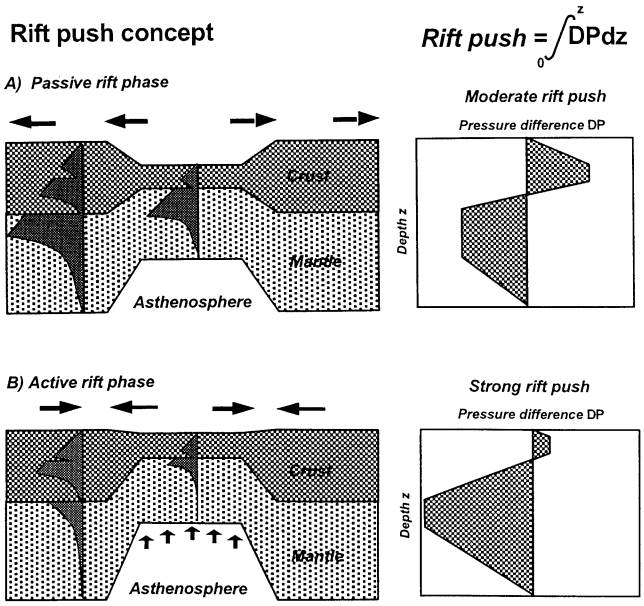

Figure 7. Rift push and twostage extension of the lithosphere. Enhanced rift push due small-scale convective upwelling may generate second phase of extension. (a) Passive rifting generates moderate extensional rift push force of the order of 1. x 10^{12} N m^{-1}. (b) Subsequent small-scale convective upwelling of the mantle lithosphere beneath the rift basin results in a dramatic increase of the rift push force of the order of plate boundary forces, i.e., 2. x 10^{12} N m^{-1}.

Here $\Delta e_i^{\text{plastic}}$ is the plastic strain increment in principal stress directions, and λ_s is the plastic multiplier. An expression for λ_s can be derived using equation (10) and the condition that $F = 0$ after plastic yield

$$\lambda_s = \frac{F^*}{A - BN_\Psi - BN_\Phi + AN_\Psi N_\Phi}. \tag{12}$$

Here $A = (K + 4G/3)$, and $B = (K - 2G/3)$, K is the elastic bulk modulus, G is the elastic shear modulus, and F^* is the predicted yield. The stresses update rule due to plastic relaxation in principal stresses has the form

$$\begin{aligned} \sigma_1 &= \sigma_1 - \lambda_s(A - BN_\Psi) \\ \sigma_3 &= \sigma_3 - \lambda_s(B - AN_\Psi). \end{aligned} \tag{13}$$

The algorithm for Mohr-Coulomb plastic yielding can be summarized in the following steps: (1) transform normal stress tensor to principal stresses, (2) check yield criterion F (equation (9)), (3) if F <0, then calculate λ_s (equation (12)), (4) update principal stresses (equation (13)), and (5) transform principal stress tensor to normal stresses.

Update of the stresses according to this scheme is performed every time step, resulting in a stress state satisfying the Mohr-Coulomb criterion throughout the computational domain. The advantage of using Mohr Coulomb plasticity is that dynamic pressure variations due to tectonic stresses affect failure and amplify the tendency for localization, which more resembles the brittle behavior of rocks then when using a pressure-independent von Mises-type yield criterion. Thus the above described algorithm realizes the viscoelastoplastic rheology and fulfils the stress equilibrium (equation (2)).

Because we are studying time-dependent phenomena, the accuracy of our numerical code is important. Our time discretization is fully implicit, which implies stability, and is second-order accurate. We chose a time step which is typically $\Delta t \leq 0.1$ of the dynamically chosen Courant time step. Decreasing time step size further does not significantly change the results.

The temperature distribution should be computed at each stage of the model evolution since powerlaw creep is a strong function of temperature and the lateral and vertical variations of temperature induce buoyancy forces through the temperature dependence of density. The 2-D temperature field in the model is obtained by solving the time dependent heat diffusion equation [*Turcotte and Schubert,* 1982]:

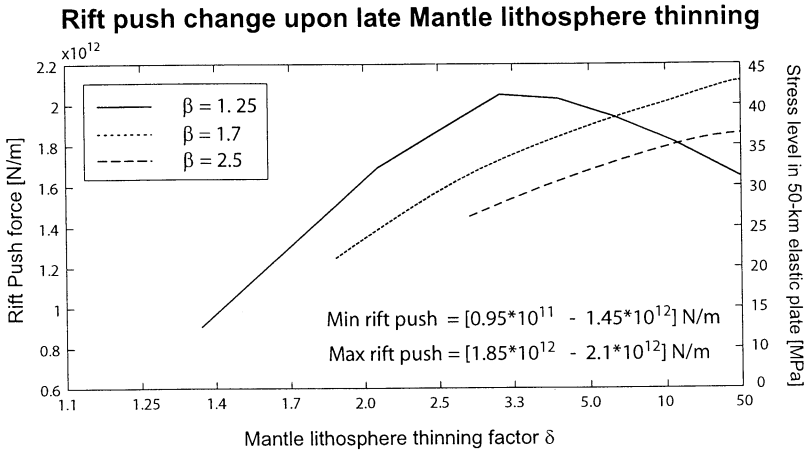

Figure 8. Increase of buoyancy force owing to late mantle lithosphere thinning. For parameters used see Figure (6). β and δ are crust and mantle lithosphere thinning factors respectively, note non-linear scale for mantle thinning factor.

Table 2. Parameters Used

Symbol	Meaning	Value
E	Youngs modulus	10^{10} Pa
G	shear modulus	10^{10} Pa
ν	Poisson ratio	0.25
n_G	wet granite	3.3
Q_G	creep	186.5 kJ mole^{-1}
A_G	parameters	3.16 x 10^{-26}Pa$^{-3.3}$ s^{-1}
n_D	dry diabase	3.05
Q_D	creep	276 kJ mole^{-1}
A_D	parameters	3.2 x 10^{-20}Pa$^{-3.05}$ s^{-1}
n_O	dry olivine	3.0
Q_O	creep	510 kJ mole^{-1}
A_O	parameters	7 x 10^{-14}Pa$^{-3.0}$ s^{-1}
ϕ	angle of friction	30°
ψ	angle of dilatation	0°
S_0	cohesion	2 x 10^6Pa
ρ_{uc0}	density U-crust 0°C	2700 kg m^{-3}
ρ_{lc0}	density L-crust 0°C	2800 kg m^{-3}
ρ_{m0}	density Mantle 0°C	3300 kg m^{-3}
α	thermal expansion	3.1 x 10^{-5}°C^{-1}
k	thermal conductivity	2.6 W m^{-1} °C^{-1}
c_p	specific heat	1050 m^2 s^{-2} °C^{-1}
H	heat production	1.10^{-6}W m^{-2}

$$\rho C_p \frac{\partial T}{\partial t} = \nabla(k\nabla T) + H, \tag{14}$$

where ρ is the density, C_p is the specific heat, T is the temperature, t is time, k is the conductivity, and H is the heat production per unit volume. The solution to this equation is found using a separate finite element code that uses the same geometry as the mechanical one. As the thermal field is advected by the displacements of the mechanical grid, the advection term does not appear in the heat equation. In most slow-flow problems it is justified to solve the mechanical and thermal equations sequentially since changes in geometry and temperature are small on the timescale of order of thousands of years. The time step should be taken small enough to justify this uncoupling of the set of partial differential equations. Thermal boundary conditions include fixed temperatures at the surface and the bottom boundary of the model and zero lateral heat flux through the side boundaries. The temperature dependence of density is included in the form

$$\rho = (1 - \alpha_T T)\rho_0, \tag{15}$$

where ρ_0 is the density at 0°C and α_T is the coefficient of thermal expansion.

4. Numerical Model Formulation and Setup

End-member crust and lithosphere configurations are used for the initial model geometry. Lithosphere thinning and extensional basin formation occur predominantly along preexisting major weakness zones in the crust as well as in the lithosphere [*Dunbar and Sawyer,* 1988; *Boutilier and Keen,* 1994]

Therefore the two chosen model end-member configurations, e.g., initial thick crust and normal lithosphere or homogeneous crust with a thermally perturbed mantle lithosphere, may be seen as abstractions of end-member prerift configurations. Since variations in crust and lithosphere structure occur primarily across continental rifts as well as passive continental margins, it is in a first approach valid to model lithosphere extension in a 2-D vertical section through the lithosphere deforming in plane strain.

We used 3600, seven-node isoperimetric triangular elements with a 13-point Gauss integration scheme. Figure 9 shows the configuration of our model, which is 1000 km wide and 120 km thick. This thickness corresponds roughly to isotherms at the base of the lithosphere, ranging from 1000°C to 1300°C. The model is fixed at the bottom in the vertical direction and free to

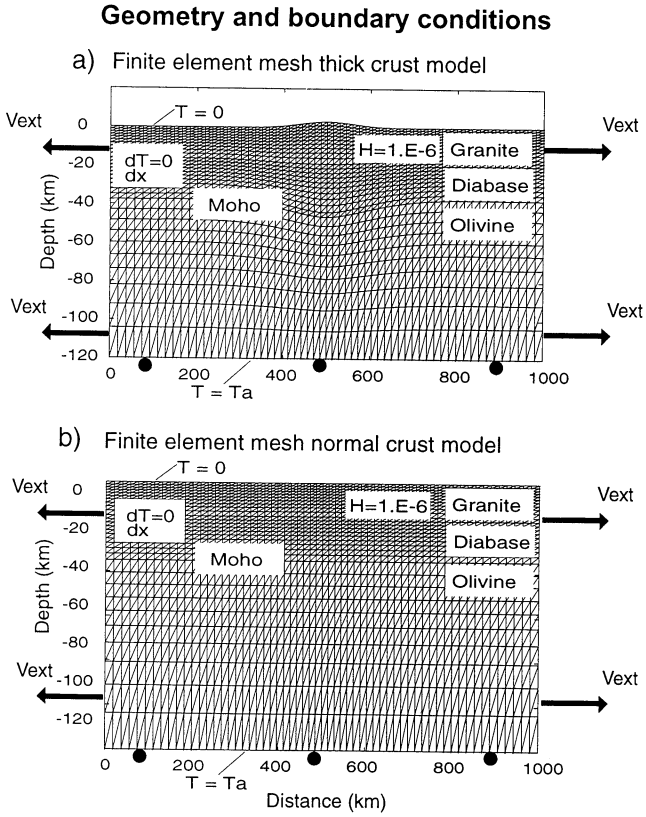

Figure 9. Mesh and boundary conditions for the finite element models. (a) Models of thick crust, characterized by a 200-km-wide zone of 40-km-thick crust and no or only a small thermal perturbation of 50°C at the bottom of the model. (b) Models of normal crust, characterized by a constant crustal thickness of 35 km and a large thermal perturbation of 150°C at the base in the center of the model. The base of the models is fixed in the vertical directions and free to move in the horizontal one, and the upper surface is free to move. Extensional boundary velocities are applied at the lateral no-tilt boundaries.

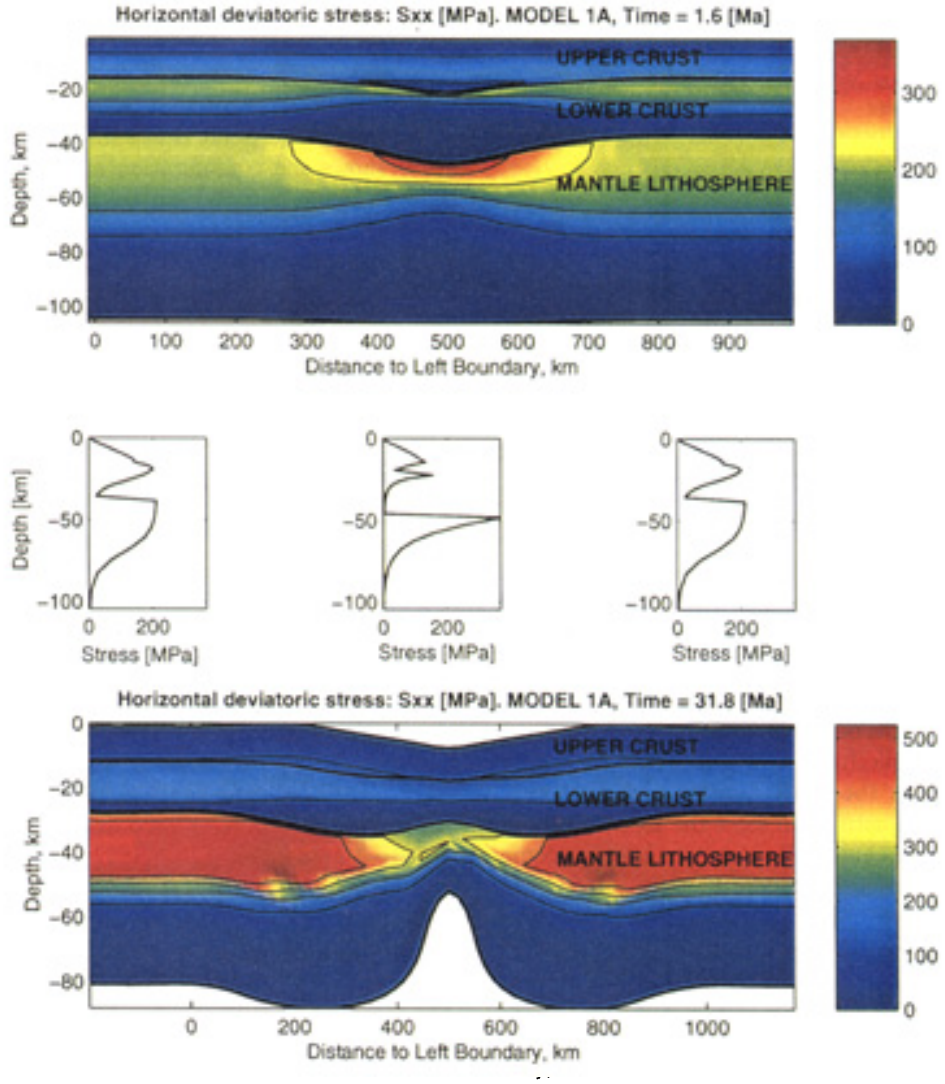

Plate 1. Model 1A thick crust, small thermal perturbation, T_a=1000°C. Stress plotted on the deformed grid (top) at 2 Myr and (bottom) at 32 Myr.

move in the horizontal direction, and the upper surface is free to move. At these temperatures creep will relax tectonic stresses in a time small compared with the geological timescale. Although the lower boundary of our models is fixed in the vertical direction, by extending our model to depths of 120-150 km a fluid layer is incorporated in the computational domain in which isostatic compensation takes place.

A constant velocity of 2 x 10^{-10} m s^{-1} is applied to the right- and left-hand side boundaries of the models. This is equivalent with a background strain rate of 4 x 10^{-16} s^{-1}. Upon localization of deformation in the 200-km-wide center of the model strain rates may go up to 2 x 10^{-15} s^{-1}. It has been pointed out that force boundary conditions may be more relevant to geological problems [*Kusznir,* 1982]. One may argue that once the lithosphere has been weakened significantly by rifting, the rate of extension will be controlled in part by resistance to motion elsewhere in the system of the plates and kinematic boundary conditions are a reasonable assumption [*Bassi et al.,* 1993]. The models are not prestressed; in the first few time steps the model is loaded only with gravitational forces which establishes a state of equilibrium.

The temperature is found with the following boundary conditions: (1) radiogenic heat is only produced in the upper crust where it is constant and equal to 1 x 10^{-6} W m^{-3}, (2) no lateral heat flux is permitted through the side boundaries, (3) the surface temperature $T_0 = 0°C$, and (4) constant temperature conditions are imposed on the lower boundary $T_a = 900°C$ (cold model), $T_a = 1000°C$ (intermediate model), and $T_a = 1300°C$ (hot model). With these assumptions the surface heat flow is within the range $40 - 120$ x 10^{-3} W m^{-2}. This is compatible with observed heat flow values typical of continental lithosphere [*Chapman,* 1986].

During the model evolution the temperature is fixed at the base of the model which remains at a constant depth. The relative importance of thermal advection and conduction is determined dynamically inside the domain and depends on the rate of upwelling, the depth range, and the thermal diffusivity. Since in general during rifting thermal advection is much more efficient then conduction (e.g., high Peclet number case), the initial thermal field is effectively contained during the model evolution. Thus the constant temperature boundary condition is only important for the initial setup of the problem and of minor influence during the model evolution.

Increased heat production owing to crustal thickening increases the geothermal gradient in the center of the thick crust models. This may result in a thermal anomaly of the order of 50°C at depths comparable to the thickness of the lithosphere. Since we choose to use a Dirichlet boundary condition at the base of the models (e.g., constant temperature), we apply a thermal anomaly of 50°C at the base of the thick crust models to keep the thermal structure consistent with the increase heat production.

5. Numerical Results

5.1. Models With Thickened Crust

This set of models is characterized by a 350-km-wide zone of thermally relaxed crust, thickened by 10 km with respect to the reference crustal thickness of 35 km (Figure 9a). The mantle lithosphere has a constant thickness of 120 km. A Gauss-shaped small thermal perturbation with a maximum of 50°C is applied in the center at the base of the lithosphere. The crust is composed of two layers, quartzite for the upper 15 km, diabase from 15 to 35 km, and the mantle lithosphere is following an olivine rheology.

5.1.1. Model 1A, thick crust, small thermal perturbation. The model is characterized by a basal temperature of $T_a = 1000°C$ with a thermal anomaly of $\Delta T = 50°C$. Plate 1 shows horizontal deviatoric stress τ_{xx} plotted on the deformed geometry of the model, depth sections of τ_{xx} at chosen localities at 2 Myr and 32 Myr. Most of the thermal anomaly in this model is due to the increased heat production in the thickened region .

Stress concentration takes place in the upper part of the mantle lithosphere and in the upper and middle crust. Deformation takes place in a combination of plastic and ductile flow. The upper part of the crust can be seen to follow Byerlee's law for frictional sliding. In the lower crust and the lower mantle lithosphere low viscosity zones are visible (Plate 1) deformation essentially takes place by viscous creep. The higher geothermal gradient together with depressing the Moho to a greater depth reduces the depth range of strong mantle lithosphere and stress concentration takes place in the upper part of the mantle lithosphere. The strength of the lower crust in the thickened region has been reduced significantly, and a low-viscosity zone can be observed in the lower part of the upper crust. In the following stages of the model run, localization of deformation will take place in the center part of the region.

At 32 Myr (Plate 1 bottom) after 350 km extension, the rift is in its mature stage. A broad basin developed. Moderate thinning of the crust is in contrast with very high thinning of the mantle lithosphere. Small-scale convection beneath the rift zone has been effective in redistributing the mass beneath the rift zone and in producing additional thinning of the mantle lithosphere. Thickened regions in the lower crust and in the lower mantle lithosphere can be observed beneath the flanking regions. Significant thermal advection has occurred beneath the rift zone.

In Figure 10, details of basin subsidence, asthenosphere uplift, and thinning history are given. Fast subsidence of the basin center to a maximum depth of 7.5 km occurred in the first 10 Myr. Subsequently, the basin

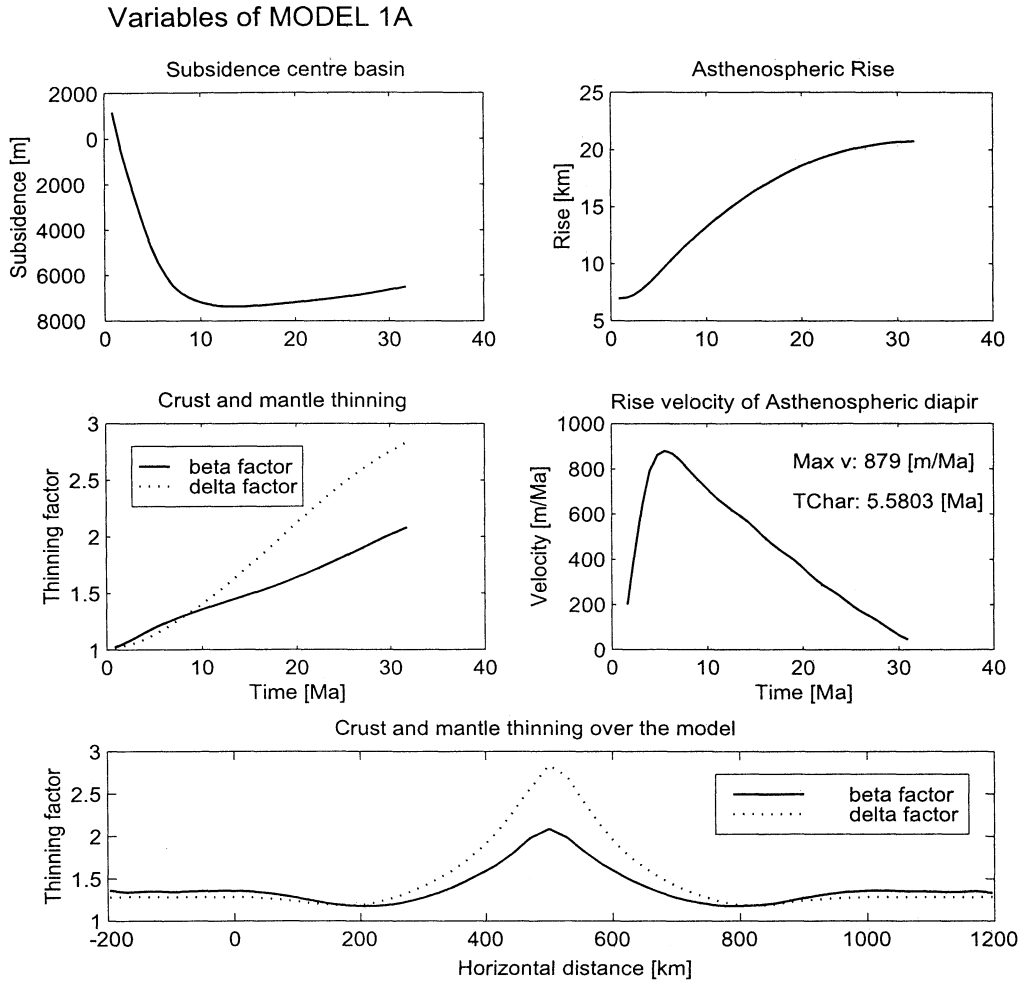

Figure 10. Model 1A, (top) subsidence and rise of the asthenosphere in the center of the model, (middle) β and δ in the center of the rift zone and rise velocity of the asthenosphere, and (bottom) β and δ over rift zone. Thinning factors for the crust and mantle lithosphere β and δ are defined as the ratio between the initial and the final thickness of the respective layer.

floor was slightly uplifted to shallower depths. Rise of the asthenosphere beneath the basin occurred over a longer time period of 30 Myr.

Relative crust and mantle thinning factors, β and δ, over the model at 27 Myr show strong differential thinning in the center of the model. Crustal thinning is distributed over an area of 200 km, whereas strong localized diapiric upwelling of the mantle lithosphere focuses mantle lithosphere thinning in a narrow zone in the center of the model.

The plot of asthenospheric rise shows that after a short initial phase the asthenosphere diapir departs from the passive uplift pattern and accelerates. A maximum rise velocity of 880 m Myr^{-1} is achieved around 5.5 Myr. After this time, the rise velocity slowly decays. The three stages shown are typical for diapir growth, e.g., a first phase of linear growth of the perturbation, followed by a phase of acceleration and nonlinear growth, and finally the reaching of a limiting boundary given by the surface or a layer with distinct lower density at which the diapir stops or extrudes. In the case considered here, the density contrast between the diapir and its surroundings is slowly decreasing, and the rheology becomes increasingly stronger with increasing uplift due to the lower temperatures at shallower depths.

5.1.2. Model 1B, effect of increasing lithosphere thickness. In this model the effect of increasing the lithosphere thickness to 150 km is studied. All other parameters remain the same as in the previous model. Keeping the same basal temperature has the effect of lowering the geothermal gradient. Therefore the models are not completely equivalent in terms of the rheology of the upper part of the system. The change of Moho temperature is, however, minor.

Mantle lithosphere upwelling is focussed in a narrower, 150-km-wide zone (Figure 11). Crustal layers have been thinned by a moderate amount of $\beta = 2$, whereas the mantle lithosphere has been thinned by a factor $\delta = 4.8$. The uplift history of the asthenosphere diapir (Figure 11) again shows the three typical stages.

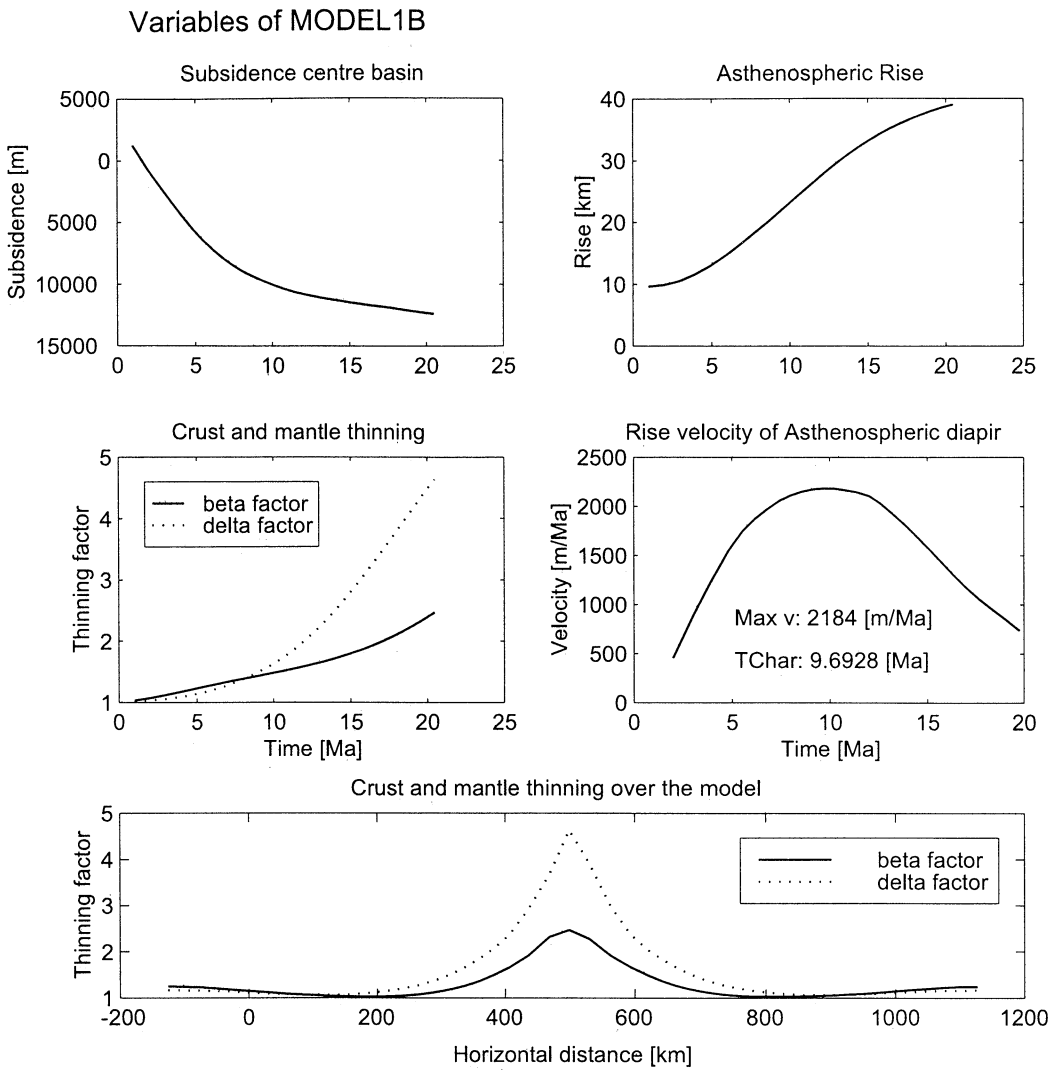

Figure 11. Effect of variation of lithosphere thickness (model 1B). Upwelling velocity and thinning factors for model with higher lithosphere thickness. The main effect is to increase the buoyancy forces. This results in higher upwelling velocity for the asthenosphere and higher total mantle thinning. Additionally, the region of upwelling is narrower then in the reference case.

At around 7 Myr, mantle thinning can be seen to depart from crustal thinning. The average asthenosphere upwelling velocity has increased in comparison to the reference model to a value of $V_{\max} = 2.2$ km Myr^{-1}. Compared with the previous model run, much higher rise velocities are reached. It may be concluded that increasing the mantle lithosphere thickness has the effect of increasing the buoyancy forces and the potential instability upon mantle lithosphere thinning. Because of the lowered geothermal conditions acceleration is, however, slowed down, and it takes more time to reach these higher velocities.

5.1.3. Effect of asthenosphere temperature. A series of runs similar in setup to models 1, with and without thermal anomaly at the base, have been performed in order to investigate the dependence of upwelling velocity on asthenosphere temperature. The basal temperature is the only variable that is varied. The results are summarized in Figures 12a and 12b.

The variation of temperature at the base of the model shows a clear dependence of maximum and average rise velocity of the asthenosphere upon the ambient temperature (Figures 12a and 12b). The average velocity is obtained by taking the average on the trajectory of steady state velocity. At low temperatures, upwelling is negligible, whereas at higher temperatures rise velocities increase strongly. Models in which the thermal anomaly is only due to increased heat production in the thickened region (curve zero T anomaly), show a more gradual increase of rise velocity than models with a thermal perturbation at the base. The increase of rise velocity with temperature may be explained by the strong dependence of viscosity on temperature and by the increased buoyancy forces.

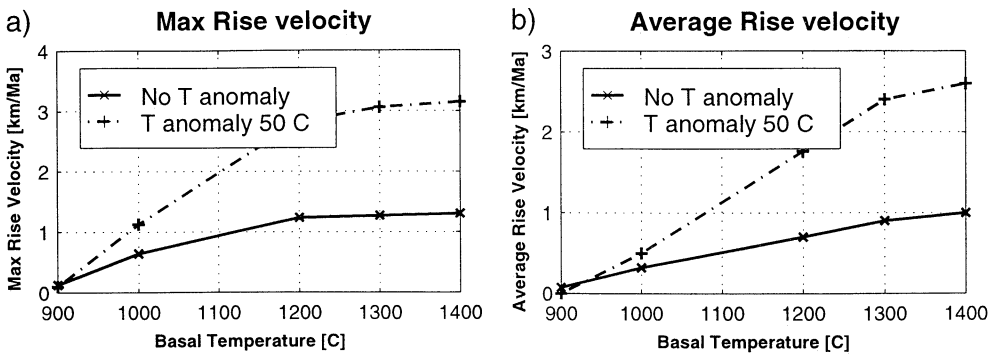

Figure 12. (a) Average rise velocity versus asthenosphere temperature. (b) Maximum rise velocity versus asthenosphere temperature.

5.1.4. Conclusions from models with thickened crust. The main difference between the models with and without thermal anomaly is given by the timescales and velocities of diapiric upwelling beneath the basin. This is mainly due to the larger buoyancy force and the focusing effect resulting from the thermal anomaly at the base in the central part of the model.

In the case of initial thickened crust and no or minor thermal perturbation of the mantle lithosphere, thinning of the crustal layer occurs in a much wider zone then mantle lithosphere thinning. This is in agreement with the results of *Buck* [1991], which show that increasing the ability of the lower crust to flow in response to crustal thickness variations, may decrease the ability of the crust to fail in a localized way, resulting in a wide rift.

The results here show that wide rifting of the crustal layer does not necessarily imply wide rifting of the mantle lithosphere. On the contrary, narrow mantle lithosphere upwelling may be significant below a wide rift. This may be explained by the fact that mantle thinning is not only driven by the far-field necking instability but also by the small-scale convective buoyancy instability. Thus, in the case of thick crust with a large amount of low viscous lower crust, the buoyancy instability is stronger than the necking instability. This is in agreement with results by *Bassi and Bonnin* [1988], who performed a linear stability analysis on a layered viscoplastic medium in the presence of gravity and density inversion over the lithosphere asthenosphere boundary, which showed that the buoyancy-driven flow forms the dominant instability upon lithosphere thinning.

The effect of increasing basal temperature as well as lithosphere thickness in both types of models is to promote the buoyancy instability of the mantle lithosphere. The model runs show that even in the absence of a thermal anomaly at the base of the lithosphere, the thermal anomaly due to crustal thickening and due to advection upon thinning may be sufficient to drive the small-scale convective instability.

5.2. Constant Crustal Thickness, Thermally Perturbed Lithosphere Model

This model is characterized by an initial homogeneous crustal thickness and a thermally perturbed mantle lithosphere, which forms the mechanical weakness zone at which extensional deformation localizes (Figure 9b). The amount of weak lower crust is decreased compared with the previous models.

Large wavelength thermal anomalies (e.g., thickness variation of the lithosphere), exist on time-scales of 100-200 Myr. In this respect, the large wavelength thermal anomaly we apply here at the base of the model may be interpreted as representing an inherited thickness variation of the lithosphere. The anomaly we choose corresponds to a thickness variation of the lithosphere of 15 to 20 km.

Model 2 is characterized by a homogeneous crustal thickness and large thermal perturbation. The asthenosphere has an intermediate temperature of 1000°C at 120 km depth. The Gauss-shaped thermal perturbation, applied at the base of the model, now has a maximum of 150°C, resulting in a temperature of 1150°C in the center of the model.

Plate 2 shows the situation at 2 Myr and at 24.5 Myr. Horizontal deviatoric stress τ_{xx} is plotted on the deformed geometry of the finite element mesh. Deviatoric stress τ_{xx} depth sections are given for chosen localities (Plate 2, middle).

At 2 Myr, stress concentration takes place in the upper part of the mantle lithosphere and in the upper crust. Deformation takes place in a combination of plastic and ductile flow. The upper part of the crust can be seen to follow Byerlee's law for frictional sliding. In the lower crust and the lower mantle lithosphere, low-viscosity zones are visible (Plate 2, top) where deformation essentially takes place by viscous creep. Above the thermal anomaly in the center of the model, where stresses in the lower mantle lithosphere are relaxed, one can observe that due to this relaxation stress concentration takes place in the upper mantle lithosphere.

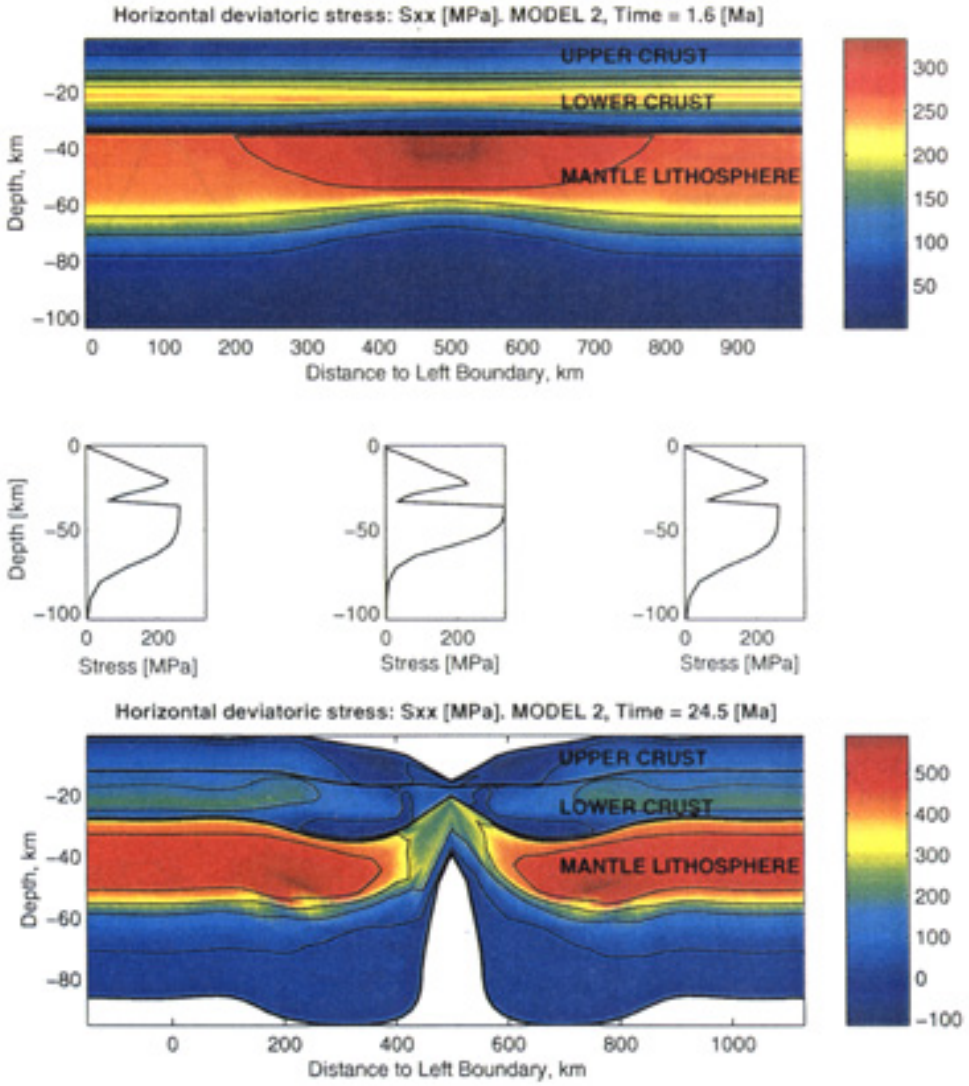

Plate 2. Model 2, constant crustal thickness, thermally perturbed mantle lithosphere, T_a=1000°C. Stress and temperature (top) at 2 Myr and (bottom) at 24.5 Myr.

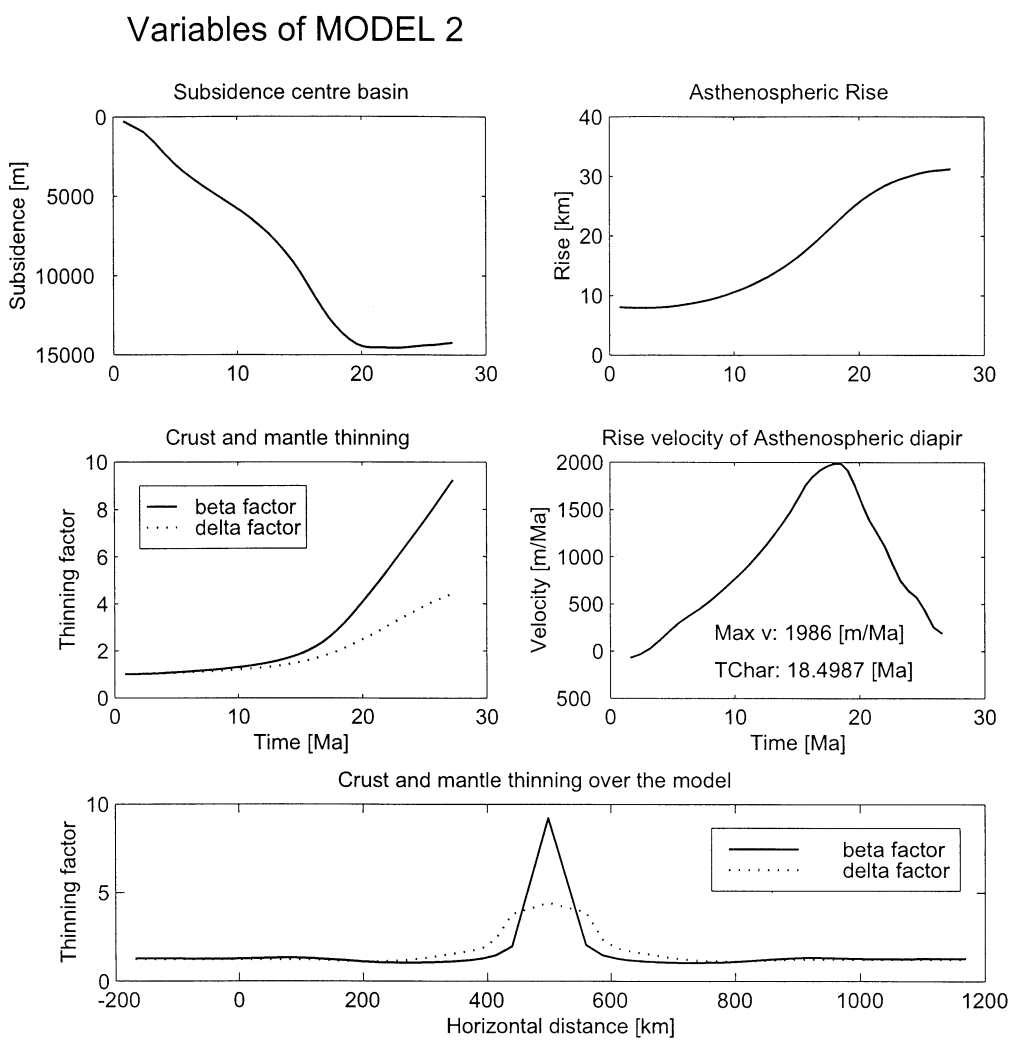

Figure 13. (top) Subsidence and rise of the asthenosphere in the center of the model, (middle) β and δ in the center of the rift zone and rise velocity of the asthenosphere (middle panels), and (bottom) β and δ over rift zone.

At 24.5 Myr (Plate 2, bottom) the rift zone is strongly developed. Interestingly, it can be observed that in the flanking regions the crust as well as the mantle are thickened in an independent way. The mantle lithosphere beneath the flanks has been thickened due to the mass redistribution by small-scale convection, and the lower crust beneath the flanking regions has been thickened due to gravity flow from the uplifted Moho in the center of the rift zone.

In Figure 13, details of the subsidence, asthenosphere uplift, and thinning history are given. The center of the basin subsided rather monotonously from 0 to 20 Myr. Relative crust and mantle thinning factors, β and δ, over the model at 27 Myr show strong differential thinning in the center of the model. Moderate strong extension of the mantle lithosphere by a factor of $\delta = 4$ is in contrast with very strong thinning of the crust by a factor of $\beta = 9$. The thinning of the crust in this model occurs over a much narrower zone than mantle lithosphere thinning leading to a much higher β factor than δ factor for the center of the rift zone.

The thickening of the mantle lithosphere beneath the flank regions shows that the small-scale convective buoyancy instability drives the localized flow in the mantle lithosphere. The strong localization in the crust is caused by the plastic instable necking in response to the strong mechanical discontinuity created by localized small-scale convective instability.

6. Phase Diagrams of Lithosphere Extension Modified for Role of Small-Scale Convection

Studies distinguishing between the different modes of rifting concentrated until now, apart from the effects of lithosphere cooling [*England,* 1983], predominantly on crustal architecture of rift basins and rifted margins [*Buck,* 1991; *Bassi et al.,* 1993]. Previous ideas on

the style of lithosphere extension may be modified for the twostage extension model developed above and for the potential of small-scale convective behavior of the mantle lithosphere. Building on the work of *Braun and Beaumont* [1987], *Buck* [1991], *Bassi et al.* [1993] and the results presented here, phase diagrams have been constructed for the dependence of the mode of rifting on crustal thickness, asthenosphere temperature, and strain rate, extending the previous results with the tendency for asthenosphere upwelling (Figures 14 and Figure 15).

These diagrams are of a necessarily qualitative nature considering the large uncertainties in thermal and rheological parameters and since a finite perturbation analysis for this system has not been developed yet. However, we think it helpful in understanding the dynamics of lithosphere extension to qualitatively discuss the first-order controls and tendencies of the system and the distinction between different modes of rifting. Although it has been demonstrated that linear perturbation analysis has only limited value for finite perturbation problems [*Buck et al.*, 1999; *Schmalholz and Podladchikov*, 2000] and is only strictly valid for infinitesimal strains, we compare the obtained large deformation results to the first-order estimates of the scaling estimates of the linear analysis [*Fletcher and Hallet*, 1983; *Zuber and Parmentier*, 1986; *Bassi and Bonnin*, 1988; *Conrad and Molnar*, 1997].

6.1. Effect of Gravity and Brittle Layer Thickness

These works [*Fletcher and Hallet*, 1983; *Bassi and Bonnin*, 1988] consider the stability of a rheologically stratified medium with alternating brittle/plastic and nonlinear stress and temperature-dependent viscous layers. Introducing the dimensionless parameter S

$$S = \frac{\rho g H_B}{2\tau_y}, \tag{16}$$

where ρ, H_B, and τ_y are density, thickness and brittle/plastic yield strength of the layer, respectively, it is shown that a necessary condition for instability is given by

$$S \leq \frac{H_B}{Z_e}, \tag{17}$$

where Z_e is the length scale for viscosity decay by a factor e. If the criterion is not met, extension is predicted to proceed stably without localized necking [*Fletcher and Hallet*, 1983]. Whereas S describes the effect of gravity, which stabilizes the system if gravity increases with depth, H_B/Z_e gives the ratio between the brittle/plastic stresses and the viscous stresses in the layer. That is, increasing brittle layer thickness increases the tendency for localized necking. The linear analysis showed that the system is very sensitive to the relative strength of the layers [*Fletcher and Hallet*, 1983; *Bassi and Bonnin*, 1988].

Using realistic parameters for lithosphere rheology and thermal structure [*Fletcher and Hallet*, 1983; *Bassi and Bonnin*, 1988] for the crust $S \sim 2.5 - 8.0$ and $H_B/Z_e \sim 4 - 8$, whereas for the mantle lithosphere values where derived of $S \sim 3.5 - 9.0$ and $H_B/Z_e \sim 10 - 12$, which shows that the crustal layer may show either stable or unstable behavior, whereas the upper mantle lithosphere appears to be unstable for most parameter values [*Fletcher and Hallet*, 1983].

For the lithosphere-asthenosphere boundary the criterion is always met since $S = (\rho_a - \rho_l)gH/2\tau_y < 0$ [*Bassi and Bonnin*, 1988]. Here the growth rate of the instability has been demonstrated [*Conrad and Molnar*, 1997] to be inversely proportional to μ_a, the asthenosphere viscosity:

$$q \sim \frac{\Delta\rho g}{\gamma\mu_a} q', \tag{18}$$

where q and q' are the dimensional and dimensionless growth rate, respectively, $\Delta\rho$ is the density contrast between lithosphere and asthenosphere, and γ is the inverse e-folding length of viscous decay. Thus increasing asthenosphere temperature decreases the viscosity and thus promotes growth of the diapiric instability. This is consistent with estimates derived elsewhere [*Huismans*, 1999] for the timescale of asthenosphere doming,

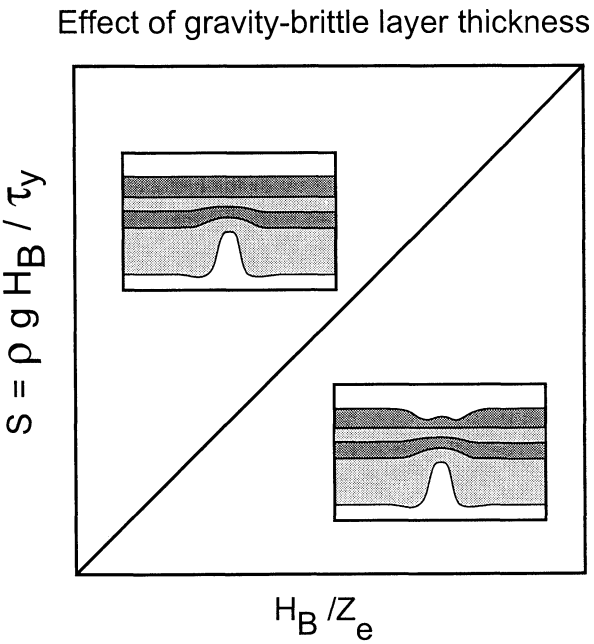

Figure 14. Summary of predictions of the linear perturbation analysis [*Fletcher and Hallet*, 1983; *Bassi and Bonnin*, 1988]. Relative importance of gravity factor S versus ratio brittleviscous stresses H_b/Z_e. S describes the effect of gravity, which is stabilizing if gravity increases with depth, whereas H_b/Z_e is related to the viscosity contrast between the unstable layer and the surrounding medium and should for stability to occur to be as great as possible. Note that for the lithosphere-asthenosphere boundary, gravity decreases with depth, and consequently, this boundary is always unstable.

which is found to depend strongly on the viscosity and temperature of the asthenosphere.

Summarizing the control of S and H_B/Z_e on the style of rifting (Figure 14), the linear theory predicts for low values of H_B/Z_e stable extension of the crustal layers, with the lithosphere-asthenosphere boundary being the most unstable interface in the system. At higher brittle layer thickness, unstable necking of the crustal layers may occur concomitant with diapiric instability of the lithosphere-asthenosphere boundary.

Qualitatively, this compares well with our results where crustal localization is sluggish or inhibited in the case of the thick crust models (e.g., low ratio of brittle to viscous stresses), whereas in the normal thickness crust model, strong plastic instabilities develop both in the crustal and upper mantle lithosphere layer, and diapiric upwarp of the asthenosphere occurs in both models.

6.2. Effect of Asthenosphere Temperature and Crustal Thickness on the Style of Extension

Thus at low asthenosphere temperature and normal crustal thickness, the diapiric tendency of the asthenosphere is low and narrow rifts may be formed. Bending stresses in the upper part of the mantle lithosphere may result in flexurally supported rift flank uplift (Figure 15a). At normal to high asthenosphere temperature and normal crustal thickness, strong localization of deformation may be expected in the mantle lithosphere as well as in the crustal layers. Crustal necking may be triggered by the strong mechanical discontinuity given by localized upwelling of the asthenosphere, resulting in more or less homogeneous thinning of mantle and crustal layers.

Increasing crustal thickness has the effect of increasing the potential for lower crustal flow in response to crustal and lithospheric thickness variations and consequently decreases the ability of the crust to deform in a localized way. Thus, on a crustal scale, extension occurs in a wide rifting mode. The mantle lithosphere, however, may show strong localized upwelling due to the buoyancy instability. Increasing the asthenosphere temperature has the effect of increasing the diapiric upwelling. Thus wide rifts with strongly thinned mantle lithosphere may result from rifting of thick crust and a moderate asthenospheric temperature. Whether, ultimately, crustal necking may accelerate and lead to breakup depends, among other factors, on the ability for the crust to localize deformation.

6.3. Effect of Asthenosphere Temperature and Strain Rate on the Style of Extension

The relative importance of asthenosphere temperature and strain rate are summarized in Figure 15b. At low strain rates and low to moderate asthenospheric temperature, the effects of thermal conduction may dominate over the effects of thermal advection. Small-scale convection in this case is not effective, since the potential for upwelling depends strongly on the size of the thermal perturbation in the lithosphere. These conditions may result in wide rift mode, with sluggish extension characterizing crust as well as mantle lithosphere thinning.

Increasing the asthenosphere temperature has the tendency to promote the buoyancy instability of the mantle lithosphere. The low strain rates, however, still facilitate cooling, and it will depend on the availability of a thermal perturbation in the system whether localized asthenosphere upwelling will occur or not. At high strain rates and low asthenospheric temperatures the diapiric instability will be suppressed, and homogeneous narrow rift mode extension of the lithosphere is expected. At high asthenosphere temperature and high strain rates, a feedback relation exists between the buoyancy instability and the necking instability of the

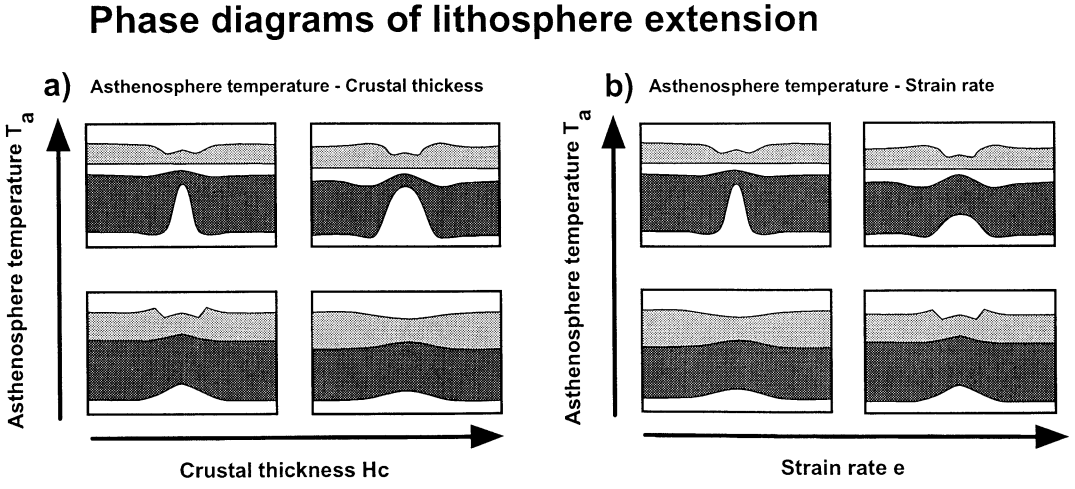

Figure 15. Phase diagrams of lithosphere extension. (a) The relative effects of asthenosphere temperature and crustal thickness on the structural style of rifting. (b) Effect of strain rate and crustal thickness on the style of rifting

crustal layers. This may result in narrow rifts in the case of normal crustal thickness and in wide rifts with localized thinning of the mantle beneath it in the case of initially thickened crust.

7. Discussion and Conclusion

Some portions of the continental lithosphere appear to be stable on long timescales and have undergone little or no deformation [*Hoffman,* 1990]. Apparently, an additional mechanism is required for it to become unstable. Other authors have suggested that thickening of the mantle lithosphere could be one such mechanism [*Houseman et al.,* 1981]. We suggest here that passive intraplate driven extension provides an alternative efficient mechanism destabilizing the lower lithosphere.

Our modeling results suggest that the inherent unstable configuration, given by the cold and dense lithosphere overlying the warm and lighter asthenosphere together with horizontal plate movements, provides the main ingredients capable of explaining the observations in rift basins. Previous studies explained the occurrence of strong differential thinning, alkaline basaltic magmatism, high heat flow values, underplating beneath passive margins associated with continental rifting, postrift doming, and related observations in terms of the interaction between mantle plumes and the lower lithosphere. The results presented here suggest that there appears no need to invoke hypothetical plume activity in explaining these observations.

The previous sections have shown that small-scale convective upwelling of the asthenosphere following a phase of passive extension might be a first-order effect overlooked in previous studies. This change from plate-mode passive extension to diapiric-mode active extension might take place in the late synrift and/or postrift evolution of extensional basins. The predicted morphology of rifting with an asthenospheric diapir penetrating the mantle lithosphere closely resembles the results obtained by kinematic passive differential stretching models [*Royden and Keen,* 1980; *Sclater et al.,* 1980; *Kooi,* 1991].

Asthenosphere upwelling provides a viable mechanism explaining a number of first-order observations in rift basins which are not explained by the existing classical models of rifting. These include the frequently observed high differential stretching, high amounts of (postrift) volcanics and underplating below rifted margins, postrift doming 10 to 60 Myr after rifting, postrift tectonic activity, lower crustal flow toward the rift flanks, and possibly the coeval occurrence of extension and contraction in the late synrift and postrift phase.

The results have shown a strong control of asthenospheric temperature and prerift lithosphere configuration on the style of rifting. Narrow rifting is predicted when extension starts from a normal crustal thickness and when the mechanical discontinuity is produced by a thermal anomaly applied at the base of the lithosphere. Wide rifting, on the other hand, is predicted when the prerift configuration is characterized by a region of thick crust. In both cases the diapiric instability of the asthenosphere appears to contribute to thinning the mantle lithosphere. In the case of a narrow rift the localization of the necking instability in the crustal layers is, during the synrift, more efficient than localization of the buoyancy instability in the mantle lithosphere. The necking instability nucleates on the strong mechanical discontinuity given by the focused asthenospheric upwelling. In the case of wide distributed thinning of the crustal layers, the buoyancy instability in the mantle lithosphere is more effective than the necking instability. In this case, strong differential thinning of the mantle lithosphere is promoted. In both cases the asthenosphere may be involved in diapiric upwelling following the synrift. Whether this is the case depends, among other factors, on the asthenosphere temperature, the size of the perturbation created by passive lithospheric thinning and the lithosphere thickness.

The modeling results predict that with a lithosphere thickness of the order 120-200 km, the wavelength of asthenospheric upwelling is in the order of 100 - 200 km. This is consistent with the estimates of linear stability analysis for wavelength-layer thickness relations, which give wavelengths of the order of 150 km using the thickness of the low viscous lower part of the lithosphere. However, increasing the thickness of the lithosphere does not increase the wavelength of the asthenospheric upwelling. This may be interpreted in terms of the effect of the increasing buoyancy force with increasing layer thickness which exerts a focusing effect on the upwelling.

The buoyancy forces associated with a first phase of homogeneous lithosphere thinning are predicted to result in tensional stress levels of the order of 50-200 MPa tending to propagate the rifting process. Small-scale convective upwelling of the asthenosphere beneath the rift basin may result in a dramatic increase of the rift-related buoyancy forces. Thinning of the mantle lithosphere is estimated to result in a rift push force $F_b \sim 2 - 3 \times 10^{12}$. For most rift basins, with a surface heat flow $q_s > 75 \times 10^{-3}$ W m^{-2}, this may be sufficient to cause a second phase of extension. This is consistent with the general observation of two stage rifting with a characteristic delay time of 5-60 Myr (Table 1 and *Ziegler,* [1994]). Additionally, the rift-related buoyancy forces generate a rift push which produces compression toward the rift-flanking regions. This may provide a mechanisms to explain the coeval occurrence of extension and contraction in regions not very far apart.

The proposed twostage extension model, where a change from plate-mode passive extension to diapiric-mode active extension might take place in the late synrift and/or postrift evolution of extensional basins, provides a viable alternative to the classical end-member models of rifting.

Acknowledgments. Adrian Lenardic, William Moore, and an anonymous reviewer are thanked for their constructive comments. R.S. Huismans was supported by the Netherlands Organisation of Scientific Research (NWO), project 751.360.003. Netherlands Research School of Sedimentary Geology publication 20010101.

References

Artyushkov, E.V., Stresses in the lithosphere caused by crustal thickness inhomogeneities, *J. Geophys. Res., 78,* 7675-7708, 1973.

Bartole, R., The North Tyrrhenean-Northern Apennines postcollisional system; constraints for a geodynamic model, *Terra Nova, 7,* 7-30, 1995.

Bassi, G., and J. Bonnin, Rheological modeling and deformation instability of lithosphere under extension, *Geophys. J. Int., 93,* 485-504, 1988.

Bassi, G., C.E. Keen, and P. Potter, Contrasting styles of rifting; models and examples from the eastern Canadian margin, *Tectonics, 12,* 639-655, 1993.

Beaumont, C., C.E. Keen, and R. Boutilier, On the evolution of rifted continental margins; comparison of models and observations for the Nova Scotian margin, *Geophys. J. R. Astron. Soc., 70,* 667-715, 1982.

Bird, P., Initiation of intracontinental subduction in the Himalaya, *J. Geophys. Res., 83,* 4975-4987, 1978.

Bois, C., Initiation and evolution of the Oligocene-Miocene rift basins of south-western Europe: Contributions of deep seismic reflection profiling, *Tectonophysics, 226,* 227-252, 1993.

Boutilier, R.R., and C.E. Keen, Geodynamic models of fault-controlled extension, *Tectonics, 13,* 439-454, 1994.

Braun, J., and C. Beaumont, Styles of continental rifting: results from dynamic models of lithosphere extension, in *Sedimentary Basins and Basin-Forming Mechanisms,* edited by C. Beaumont and A.J. Tankard, pp. 241-258, Can. Soc. of Petr. Geol., Calgary, Alberta, 1987.

Buck, W.R., When does small-scale convection begin beneath oceanic lithosphere?, *Nature, 313,* 775-777, 1985.

Buck, W.R., Small scale convection induced by passive rifting; the cause for uplift of rift shoulders, *Earth Planet. Sci. Lett., 77,* 362-372, 1986.

Buck, W.R., Modes of continental lithosphere extension, *J. Geophys. Res., 96,* 20,161-20,178, 1991.

Buck, W.R., L.L. Lavier, and A.N.B. Poliakov, How to make a rift wide, *Philos. Trans. R. Soc. London, 357,* 671-693, 1999.

Carter, N.L., and M.C. Tsenn, Flow properties of continental lithosphere, *Tectonophysics, 136,* 27-63, 1987.

Chapman, D.S., Thermal gradients in the continental crust, in *The Nature of the Lower Continental Crust,* edited by J.B. Dawson, D.A. Carswell, J. Hall, and K.H. Wedepohl, *Geol. Soc. Spec. Publ., 24,* 63-70, 1986.

Cloetingh, S., and R. Wortel, Stress in the Indo-Australian plate, *Tectonophysics, 132,* 49-67, 1986.

Cloetingh, S., J.D. van Wees., P.A. van der Beek, and G. Spadini, Extension in convergent regimes: constrains from thermomechanical modeling of Alpine/Mediterranean basins and intracratonic rifts, *Mar. Pet. Geol., 12,* 793-808, 1995.

Coblentz, D.D., R.M. Richardson, and M. Sandiford, On the gravitational potential of the Earth's lithosphere, *Tectonics, 13,* 929-945, 1994.

Conrad, C.P., and P. Molnar, The growth of Rayleigh-Taylor instabilities in the lithosphere for various rheological and density structures, *Geophys. J. Int., 129,* 95-112, 1997.

Cundall, P.A., and M. Board, A microcomputer program for modeling large-strain plasticity problems, in *Numerical Methods in Geomechanics,* edited by G. Swoboda, pp. 2101-2108, A.A. Balkema, Brookfield, Vt., 1988.

Davies, P.M., Continental rift structures and dynamics with reference to teleseismic studies of the Rio Grande and East African rifts, *Tectonophysics, 197,* 309-325, 1991.

Delvaux, D., R. Moeys, G. Stapel, C. Petit, K. Levi, A. Miroshnichenko, V. Ruzhich, and V. San'kov, Paleostress reconstructions and geodynamics of the Baikal region, central Asia, Part II, Cainozoic rifting, *Tectonophysics, 282,* 1-38, 1997.

de Ruig, M.J., Tectono-sedimentary evolution of the Prebetic fold belt of Alicante (SE Spain), Ph.D. thesis, 208 pp., Vrije Univ., Amsterdam, 1992.

Dunbar, J.A., and D.S. Sawyer, Continental rifting at preexisting lithospheric weaknesses, *Nature, 333,* 450-452, 1988.

England, P., Constraints on extension of continental lithosphere, *J. Geophys. Res., 88,* 1145-1152, 1983.

Fleitcut, L., and C. Froidevaux, Tectonics and topography for a lithosphere containing density heterogeneities, *Tectonics, 1,* 21-56, 1982.

Fletcher, R.C., and B. Hallet, Unstable extension of the lithosphere: A mechanical model for Basin-and-Range structure, *J. Geophys. Res., 88,* 7457-7466, 1983.

Hamilton, W., Crustal extension in the Basin and Range province, southwestern United States, in *Continental Extensional Tectonics,* edited by M.P. Coward, J.F. Dewey, and P.L. Hancock, *Geol. Soc. Spec. Publ., 28,* 155-176, 1987.

Heeremans, M., B.T. Larsen, and H. Stel, Paleostress reconstruction from kinematic indicators in the Oslo Graben, southern Norway: New constraints on the mode of rifting, *Tectonophysics, 266,* 55-79, 1996.

Hoffman, P.F., Geological constraints on the origin of the mantle root beath the Canadian shield, *Philos. Trans. R. Astron. Soc. London, 331,* 523-532, 1990.

Horvath, F., Towards a mechanical model for the formation of the Pannonian Basin, *Tectonophysics, 226,* 333-357, 1993.

Horvath, F., and S.A.P.L. Cloetingh, Stress-induced latestage subsidence anomalies in the Pannonian basin, *Tectonophysics, 266,* 287-300, 1996.

Houseman, G., and P. England, A dynamical model of lithosphere extension and sedimentary basin formation, *J. Geophys. Res., 91,* 719-729, 1986.

Houseman, G.A., D.P. McKenzie, and P. Molnar, Convective instability of a thickened boundary layer and its relevance for the thermal evolution of continental convergent belts, *J. Geophys. Res., 86,* 6115-6132, 1981.

Hughes, J.R., and J. Winget, Finite rotation effects in numerical integration of rate constitutive equations arising in large deformation analysis, *Int. J. Numer. Methods Eng., 15,* 1862-1867, 1980.

Huismans, R.S., Dynamic modelling of the transition from passive to active rifting, application to the Pannonian basin, Ph.D. thesis, 196 pp., Vrije Univ., Amsterdam, 1999.

Illies, J.H., and G. Greiner, Rhinegraben and the Alpine system, *Geol. Soc. Am. Bull., 89,* 770-782, 1978.

Janssen, M.E., M. Torne, S.A.P.L. Cloetingh, and E. Banda, Pliocene uplift of the eastern Iberian margin: inferences from quantitative modeling of the Valencia through, *Earth Planet. Sci. Lett., 119,* 585-597, 1993.

Karner, G.D., S.E. Egan, and J.K. Weissel, Modelling the tectonic development of the Tucano and Sergipe-Alagoas rift basins, Brazil, *Tectonophysics, 215,* 133-160, 1992.

Keen, C.E., The dynamics of rifting; deformation of the

lithosphere by active and passive driving forces, *Geophys. J. R. Astron. Soc., 80,* 95-120, 1985.

Keen, C.E., and R.R. Boutilier, Lithosphere-Asthenosphere interactions below rifts, in *Rifted Ocean-Continent Boundaries,* edited by E. Banda, pp. 17-30, Kluwer Acad., Norwell, Mass., 1995.

Keen, C.E., R.C. Courtney, S.A. Dehler, and M.C. Williamson, Decompression melting at rifted margins; comparison of model predictions with the distribution of igneous rocks on the eastern Canadian margin, *Earth Planet. Sci. Lett., 121,* 403-416, 1994.

Kooi, H., Tectonic modelling of extensional basins: the role of lithospheric flexure, intraplate stress and relative sealevel change, Ph.D. thesis, 183 pp., Vrije Univ., Amsterdam, 1991.

Kooi, H., S. Cloetingh, and J. Burrus, Lithospheric necking and regional isostasy at extensional basins, 1, Subsidence and gravity modelling with an application to the Gulf of Lions Margin (SE France), *J. Geophys. Res., 97,* 17,553-17,572, 1992.

Kusznir, N.J., Lithosphere response to externally and internally derived stresses: a viscoelastic stress guide with amplification, *Geophys. J. R. Astron. Soc., 70,* 399-414, 1982.

Kusznir, N.J., and R.G. Park, Intraplate lithosphere strength and heat flow, *Nature, 299,* 540-542, 1982.

Latin, D.M., and F.G. Waters, Melt generation during rifting in the North Sea, *Nature, 351,* 559-562, 1991.

Le Pichon, X., and F. Alvarez, From stretching to subduction in back arc regions: dynamic considerations, *Tectonophysics, 102,* 343-357, 1984.

Marechal, J.C., Mechanisms of uplift preceding rifting, *Tectonophysics, 94,* 51-66, 1983.

McKenzie, D., Some remarks on the development of sedimentary basins, *Earth Planet. Sci. Lett., 40,* 25-32, 1978.

Morgan, P., and J.H. Sass, Thermal regime of the continental lithosphere, *J. Geol., 1,* 143-166, 1984.

Poliakov, A. and Y.Y. Podladchikov, Diapirism and topography, *Geophys. J. Int., 109,* 553-564, 1992.

Royden, L., and C.E. Keen, Rifting process and thermal evolution of the continental margin of eastern Canada determined from subsidence curves, *Earth Planet. Sci. Lett., 51,* 343-361, 1980.

Royden, L., F. Horvath, A. Nagymarosy, and L. Stegena, Evolution of the Pannonian Basin system; 2, Subsidence and thermal history, *Tectonics, 2,* 91-137, 1983.

Schmalholz, S.M. and Y.Y. Podladchikov, Finite amplitude folding: transition from exponential to layer length controlled growth, *Earth Planet. Sci. Lett., 179,* 355-369, 2000.

Sclater, J.G., L. Royden, F. Horvath, B.C. Burchfiel, S. Semken, and L. Stegena, The formation of the intraCarpathian basins as determined from subsidence data, *Earth Planet. Sci. Lett., 51,* 139-162, 1980.

Sengor, A.M.C., and K. Burke, Relative timing of rifting and volcanism on Earth and its tectonic applications, *Geophys. Res. Lett., 5,* 419-421, 1978.

Steckler, M.S., Uplift and extension at the Gulf of Suez: Indications of induced mantle convection, *Nature, 317,* 135-139, 1985.

Turcotte, D.L., and S.H. Emerman, Mechanisms of active and passive rifting, *Tectonophysics, 94,* 39-50, 1983.

Turcotte, D.L., and G. Schubert, *Geodynamics: Applications of Continuum Physics to Geological Problems,* 450 pp., John Wiley, New York, 1982.

van Wees, J.D., R.A. Stephenson, S.M. Stovba, and V.A. Shymanovskyi, Tectonic variation in the Dniepr–Donets Basin from automated modeling of backstripped subsidence curves, *Tectonophysics, 268,* 257-280, 1997.

Vitorello, I., and H.N. Pollack, On the variation of continental heat flow with age and the thermal evolution of continents, *J. Geophys. Res., 85,* 983-995, 1980.

Weijermars, R., Geology and tectonics of the Betic Zone, SE Spain, *Earth Sci. Rev., 31,* 153-236, 1991.

White, R.S., The Earth's crust and lithosphere, *J. Petrol., 29,* 615-624, 1988.

White, R., and D. McKenzie, Magmatism at rift zones; the generation of volcanic continental margins and flood basalts, *J. Geophys. Res., 94,* 7685-7729, 1989.

Wilson, M., Magmatism and the geodynamics of basin formation, *Sediment. Geol., 86,* 5-29, 1993.

Wilson, M., Z.M. Lyashkevich, Magmatism and the geodynamics of rifting of the Pripyat-Dnieper-Donets rift, East European Platform, *Tectonophysics, 268,* 65-81, 1996.

Ziegler, P.A., North Sea rift system, *Tectonophysics, 208,* 55-76, 1992.

Ziegler, P.A., Geodynamic processes governing development of rifted basins, in *Geodynamic Evolution of Sedimentary Basins,* edited by F. Roure, N. Ellouz, V.S. Shein, and I.I. Skvortsov, 19-67 pp., Technip, Paris, 1994.

Ziegler, P.A., Cenozoic rift system of western and central Europe; an overview, *Geol. Mijnbouw, 73,* 99-127, 1995.

Zorin, Y.A., An example of intrusion of asthenospheric material into the lithosphere as the cause of the disruption of lithospheric plates, *Tectonophysics, 73,* 91-104, 1981.

Zuber, M.T., and E.M. Parmentier, Lithospheric necking: a dynamic model for rift morphology, *Earth Planet. Sci. Lett., 77,* 373-383, 1986.

S.A.P.L. Cloetingh, Institute of Earth Sciences, Vrije Universiteit, de Boelelaan 1085, 1081 HV Amsterdam, Netherlands. (cloeting@geo.vu.nl)

R.S. Huismans, Department of Oceanography, Dalhousie University, Halifax, Nova Scotia, B3H 4J1, Canada. (ritske.huismans@Dal.Ca)

Y.Y. Podladchikov, Geologisches Institut, ETH-Zentrum, Sonnegstrasse 5, Zurich, CH 8092, Switzerland. (yura@erdw.ethz.ch)

(Received April 5, 2000; revised October 4, 2000;
accepted November 16, 2000.)

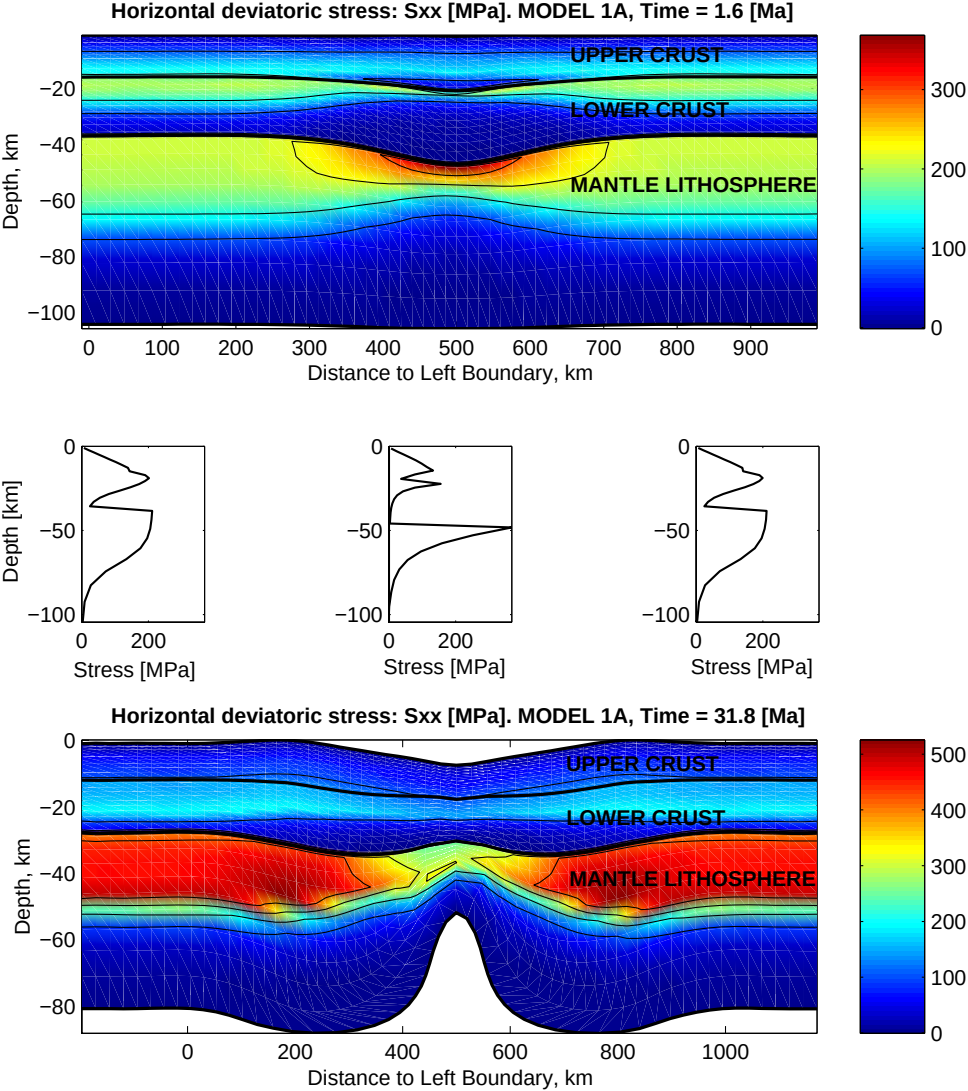
Horizontal deviatoric stress: Sxx [MPa]. MODEL 1A, Time = 1.6 [Ma]
UPPER CRUST
LOWER CRUST
MANTLE LITHOSPHERE
Depth, km
−20
−40
−60
−80
−100
0
100
200
300
400
500
600
700
800
900
Distance to Left Boundary, km
300
200
100
0
Depth [km]
−50
Stress [MPa]
Horizontal deviatoric stress: Sxx [MPa]. MODEL 1A, Time = 31.8 [Ma]
UPPER CRUST
LOWER CRUST
MANTLE LITHOSPHERE
Depth, km
−20
−40
−60
−80
0
200
400
600
800
1000
Distance to Left Boundary, km
500
400
300
200
100
0